

THESIS FOR THE DEGREE OF DOCTOR OF PHILOSOPHY

From Noise-Shaped Coding to Energy Efficiency
- *One bit at the time.*

ULF GUSTAVSSON



Microwave Electronics Laboratory
Department of Microtechnology and Nanoscience (MC2)
Chalmers University of Technology
Göteborg, Sweden, 2011

From Noise-Shaped Coding to Energy Efficiency
- One bit at the time.
ULF GUSTAVSSON

© Ulf Gustavsson
Göteborg, 2011
ISBN 978-91-7385-617-1

Doktorsavhandlingar vid Chalmers tekniska högskola
Ny serie Nr. 3298
ISSN 0346-718X

Microwave Electronics Laboratory
Department of Microtechnology and Nanoscience (MC2)
Technical report MC2-203
ISSN 1652-0769

Chalmers University of Technology
Department of Microtechnology and Nanoscience (MC2)
Chalmers University of Technology
SE-412 96 Göteborg, Sweden
Phone: +46 (0) 31 772 1000

Printed by Chalmers Reproservice
Göteborg, Sweden 2011

Till Linnéa.

Abstract

Three parameters that drive the research and development of future RF transmitter technologies for high speed wireless communication today are energy efficiency, flexibility and reduction of the physical footprint. This thesis treats the use of single-bit quantization in conjunction with a method called Noise-Shaped Coding (NSC), as an enabler for these parameters, foremost in terms of energy efficiency.

The first part of the thesis provides a short introduction to the common Radio Frequency Power Amplifier (RFPA) power efficiency enhancement techniques. The pulsed RF transmitter is introduced in which the RFPA is used as a switch, modulated by a single-bit quantized signal which allows it to operate solely at its two most efficient states.

The second part of the thesis provides an introduction to the concept of NSC and the underlying idea of how high signal quality can be achieved with one bit quantization of the signal amplitude. A particular method of implementing NSC, namely the $\Sigma\Delta$ -modulator, is introduced and some common methods for design and analysis are discussed. An optimization-based approach to $\Sigma\Delta$ -modulator design is proposed and benchmarked against conventional methods in terms of its ability to shape the power spectral density of the quantization noise according to a given reconstruction filter response, minimizing the reconstructed error metric.

The third and final part of the thesis focuses specifically on the application of $\Sigma\Delta$ -modulation in a pulsed RF transmitter context. The concepts of band-pass and baseband $\Sigma\Delta$ -modulation are introduced. A few important challenges related to the use of $\Sigma\Delta$ -modulation in a pulsed RF-transmitter context are identified. A $\Sigma\Delta$ -modulator topology which handles a complex input signal is investigated in great detail and advantages compared to conventional methods for using $\Sigma\Delta$ -modulation are unveiled by means of theoretical analysis and simulations. A method for suppressing the quantization noise within a frequency band surrounding the modulated RF carrier, enabling the use of more wideband reconstruction filter and moderate pulse-rates, is also presented. A detailed theoretical analysis reveals how optimized Noise-Shaped Coding, as provided by the optimization method introduced in the second part, can be deployed in order to improve the system performance. Finally, the method is validated by experimental measurements on two different high efficiency RFPAs at 1 and 3.5 GHz respectively, showing promising results.

Keywords: Quantization, $\Sigma\Delta$ -Modulation, Noise-Shaped Coding, Radio Frequency Power Amplifiers, Pulsed Transmitter Architectures.

List of Publications

Appended Publications

This thesis is based on work contained in the following papers:

- I. U. Gustavsson, T. Eriksson and C. Fager
"Quantization Noise Minimization in $\Sigma\Delta$ -modulation based RF Transmitter Architectures," *IEEE Transactions on Circuits and Systems I: Regular Papers*, vol. 57, no. 12, pp. 3082-3091, 2010.
- II. U. Gustavsson, T. Eriksson, H.M. Nemati, P. Saad, P. Singerl and C. Fager
"An RF Carrier Bursting System using Partial Quantization Noise Cancellation," To appear in *IEEE Transactions on Circuits and Systems I: Regular Papers*.
- III. U. Gustavsson, T.Eriksson, J.C. Pedro, P. Singerl and C. Fager
"On $\Sigma\Delta$ -Modulation of Quadrature Signals," Submitted to *IEEE Transactions on Circuits and Systems I: Regular Papers*.
- IV. N.V. Silva, A.S.R. Oliveira, U. Gustavsson and N.B. Carvalho
"A Novel All-Digital Multichannel Multimode RF Transmitter Using $\Sigma\Delta$ -modulation," Submitted to *IEEE Microwave and Wireless Components Letters*.

Other Publications

The following papers have been published but are not included in the thesis. Their content partially overlap with the appended papers or are out of the scope of this thesis.

- [a] U. Gustavsson, T. Eriksson and C. Fager "A General Method for Pass-band Quantization Noise Supression in Pulsed Transmitter Architectures," in *IEEE MTT-S International Microwave Symposium Digest*, pp. 1529-1523, June, 2009.
- [b] U. Gustavsson "Quantization and Noise-Shaped Coding for High Efficiency Transmitter Architectures," Licentiate thesis, Department of Microtechnology and Nanoscience, Chalmers University of Technology, ISSN 1652-0769; nr 146, May, 2009.
- [c] B. Berglund, U. Gustavsson, J. Thorebäck and T. Lejon "RBS High Efficiency Power Amplifier Research - Challenges and Possibilities," in *Advances in Analogue Circuit Design*, Lund 2009. Springer Press
- [d] C. Fager, H.M Nemat, U. Gustavsson, R. Jos and H. Zirath "Evaluation of high efficiency PAs for use in supply- and load-modulation transmitters," in *IEEE Topical Symposium on Power Amplifiers for Wireless Communications*, 2009.
- [e] U. Gustavsson, T. Eriksson and C. Fager "Noise-Shaped Coding and Quantization Noise Suppression for Pulsed Transmitter Architectures," RFMTC, Gävle 2009
- [f] H.M. Nemat, C. Fager, U. Gustavsson, R. Jos and H. Zirath "Design of Varactor-Based Tunable Matching Networks for Dynamic Load Modulation of High Power Amplifiers," in *IEEE Transactions on Microwave Theory and Techniques*, Issue 57, pp. 1110-1118, 2009.
- [g] U. Gustavsson, T. Eriksson and C. Fager "A method for quantization noise suppression in pulsed transmitter architectures," *Provisional patent application*, Application number 61119400.
- [h] H.M. Nemat, C. Fager, U. Gustavsson and H. Zirath "An efficiency optimized controlling scheme for dynamic load modulation of power amplifiers," in *38th European Microwave Conference Proceeding*, pp. 583-586, October, 2008.
- [i] H.M. Nemat, C. Fager, U. Gustavsson R. Jos and H. Zirath "Characterization of switched mode LDMOS and GaN power amplifiers for optimal use in polar transmitter architectures," in *IEEE MTT-S International Microwave Symposium Digest*, pp. 1505-1508, June, 2008.
- [j] H.M. Nemat, C. Fager, U. Gustavsson, F. Lepine, A. Adahl, R. Jos and H. Zirath "Practical realizations of high efficiency switched mode power amplifiers," in *German Microwave Conference*, Techn. Univ. Hamburg-Harburg, 2008.

-
- [k] U. Gustavsson, B. Almgren and H.M. Nematı "Design considerations for Varactor-based dynamic load modulation networks," in *GHz symposium*, Göteborg, Sweden, 2008.
- [l] C. Fager, H.M. Nematı, U. Gustavsson, B. Almgren, T. Lejon and H. Zirath "Voltage/Current mode class D amplifiers and their applications," in *IEEE Radio Wireless Symposium*, Orlando, FL., USA, 2008.
- [m] M. Södow, H.M. Nematı, M. Thorsell, U. Gustavsson, K. Andersson, C. Fager, P.-Å. Nilsson, J. Hassan, A. Henry, E. Janzen, R. Jos, and N. Rorsman "SiC Varactors for Dynamic Load Modulation of High Power Amplifiers," in *IEEE Electron Device Letter*, vol. 29, no. 7, pp. 728–730.
- [n] T. Eriksson, C. Fager, H. Cao, A. Soltani, U. Gustavsson, H.M. Nematı and H. Zirath "Modeling of dual-input power amplifiers," in *GHz symposium*, Göteborg, Sweden, 2008.
- [o] U. Gustavsson "Improved amplifying device," *Patent application*, PCT/SE2007/050785, filed October 26, 2007.
- [p] U. Gustavsson and R. Hellberg "A composite amplifier, a radio terminal and a method for improving the efficiency of the composite amplifier," *Patent application*, PCT/SE2007/050866, filed November 19, 2007.
- [q] C. Fager, U. Gustavsson, H.M. Nematı and H. Zirath "High Efficiency Modulation of Switched Mode LDMOS Power Amplifiers," in *11th International Symposium on Microwave and Optical Technology*, Rome, Italy, 2007.
- [r] U. Gustavsson, T. Lejon, C. Fager and H. Zirath "Design of highly efficient, high output power, L-band class D^{-1} RF power amplifier using GaN MESFET devices," in *37th European Microwave Conference Proceeding*, pp. 1089-1092, October, 2007.
- [s] N.V. Silva, A.S.R. Oliveira, U. Gustavsson and N.B. Carvalho "A Dynamically Reconfigurable Architecture Enabling All-Digital Transmission for Cognitive Radios," Accepted for presentation at *Radio and Wireless Symposium, 15-19 Jan., Santa Clara, CA, USA*

Notations and abbreviations

Mathematical Notation

$\mathbb{E}[x]$	Expected value of x
f	Frequency
f_s	Sample rate
G	Transducer gain
P_{DC}	DC power
P_{diss}	Dissipated power
P_{in}	Input power
P_{out}	Output power
$p_x(x)$	Probability density/mass function of x
R	Resistance
R_L	Resistive load impedance
R_{opt}	Optimal load resistance
R_{On}	On state resistance
\mathbb{C}	The set of complex numbers
σ_x^2	Variance of x
η	Drain Efficiency
η_c	Coding Efficiency
ω	Angular frequency
$\Phi_{xx}(\omega)$	Power Spectral Density of x
B_c	Compensation reactance
Y	Admittance
Z	Impedance
Z_L	Load impedance
Z_{opt}	Optimal load impedance

Abbreviations

ADC	Analogue to Digital Converter
ADPLL	All-Digital Phase-Locked Loop
ACPR	Adjacent Channel Power Ratio
CR	Cognitive Radio
DAC	Digital to Analogue Converter

DC	Direct Current
DCO	Digitally Controlled Oscillator
DLM	Dynamic Load Modulation
DPD	Digital Pre-Distortion
DSM	Dynamic Supply Modulation
DSP	Digital Signal Processing
DUC	Digital Up Conversion
EA	Envelope Amplifier
EER	Envelope Elimination and Restoration
ET	Envelope Tracking
EVM	Error Vector Magnitude
FET	Field Effect Transistor
GaN	Gallium Nitride
GSM	Global System for Mobile communication
HEMT	High Electron Mobility Transistor
HMM	Hidden Markov Model
HSPA	High Speed Packet Access
LDMOS	Lateral Diffusion Metal Oxide Semiconductor
LTE	Long Term Evolution
LINC	Linear amplification with Nonlinear Components
MLE	Maximum Likelihood Estimate
MLSE	Maximum Likelihood Sequence Detection
MSE	Mean Square Error
MSR	Multi-Standard Radio
NMSE	Normalized Mean Square Error
NSC	Noise-Shaped Coding
NTF	Noise Transfer Function
PA	Power Amplifier
PAE	Power Added Efficiency
PAPR	Peak to Average Power Ratio
PDF	Probability Density Function
PDM	Pulse-Density Modulation
PMF	Probability Mass Function
PPM	Pulse-Position Modulation
PWM	Pulse-Width Modulation
RAT	Radio Access Technology
RBS	Radio Base Station
RF	Radio Frequency
RFC	RF Choke
RFPA	Radio Frequency Power Amplifier
SCS	Signal Component Separator
SDR	Software Defined Radio
STF	Signal Transfer Function
SNR	Signal to Noise Ratio
SQNR	Signal to Quantization Noise Ratio
VQ	Vector Quantization
W-CDMA	Wideband Code Division Multiple Access

Contents

Abstract	v
List of Publications	vii
Notations & Abbreviations	xi
1 Introduction	1
1.1 Motivation	1
1.2 Thesis Contribution	3
1.3 Thesis outline	4
2 RF Power Amplifier Efficiency Enhancement Techniques	5
2.1 Efficiency Metrics	5
2.2 Dynamic Supply Modulation	6
2.3 Dynamic Load Modulation Techniques	8
2.3.1 The Doherty Amplifier	8
2.3.2 The Chireix Outphasing Amplifier	11
2.3.3 Varactor-based Dynamic Load Modulation	13
2.4 Pulsed RF Transmitter Architectures	16
2.4.1 RF-level Pulsed Transmitter Architectures	16
2.4.2 Baseband-level Pulsed Transmitter Architectures	17
2.5 Discussion	18
3 Noise-Shaped Coding	21
3.1 A definition of Noise-Shaped Coding	21
3.2 Noise-Shaped Coding by $\Sigma\Delta$ -Modulation	24
3.3 Design and Analysis of $\Sigma\Delta$ -modulators	24
3.3.1 The Linear Noise Model	24
3.3.2 Stability Analysis	27
3.4 A Generalized Approach to $\Sigma\Delta$ -Modulator Design	30
3.5 Discussion	32
4 $\Sigma\Delta$-Modulation for Pulsed RF Transmitters	33
4.1 RF Bandpass $\Sigma\Delta$ -Modulation	33
4.2 Baseband $\Sigma\Delta$ -Modulation	35
4.2.1 Q $\Sigma\Delta$ transmitters	35
4.2.2 P $\Sigma\Delta$ transmitters	36
4.3 Fundamental issues	37

4.3.1	Signal Reconstruction	37
4.3.2	Noise-Shaping Properties in Polar Transmitters	40
4.3.3	Concurrent Multiband Transmission	42
4.4	Discussion	44
5	Conclusions and Future Work	45
5.1	Conclusions	45
5.2	Future work	46
6	Summary of Appended Papers	47
	Acknowledgments	49
	Bibliography	51
	Appended Papers	61

Chapter 1

Introduction

1.1 Motivation

We live in remarkable times. One of the most famous quotes from the British writer and scientist Arthur C. Clarke state that "*Any sufficiently advanced technology is indistinguishable from magic.*" Being a part of one of the first generations that grew up with home-computers, running on simple 8-bit processors in the lower MHz-range of clock-frequencies, it is easy to realize that the portable technology which today is used for everyday communication would surely have appeared as somewhat magical to anyone my age back in the late 1980s. In particular, the capability of connecting to a global, world wide web and instantly being able to communicate with anyone, anywhere in the world.

What started as ARPAnet in late 1960s, [1], paved the road for the technological revolution that altered the way in which we communicate today. Paralleled by the evolution of mobile telephony, this led the world to the era of mobile broadband. The number of devices with wireless capabilities that connects to the Internet is estimated to reach 50 billions ($5 \cdot 10^{10}$) by the year 2020, [2]. It has been estimated that, during the time period of 2010-2015, the global mobile data traffic will increase 26-fold as illustrated in Fig. 1.1, and by 2015, the monthly traffic is estimated to reach 6.3 EB (Exa byte).

Access technologies such as High Speed Package Access (HSPA/HSPA+) and Long Term Evolution (LTE), [4], are deployed in order to satisfy this need for extremely high data-rates introduced by the growing amount of traffic and the large amount of connected devices. The improvements in terms of spectral efficiency commonly associated with these access technologies, introduces the need for a large dynamic range and high Peak-to-Average Power Ratio (PAPR) signals. This adds to the challenge of designing a highly efficient RF front-end. The RF power amplifier (RFPA) is a highly important building block of the RF transmitter front-end and is, in most cases, not only the largest consumer of energy in the RBS, [5], but also a significant source of nonlinearities, [6], when used with wideband, high PAPR signals. The increased amount of users and connected devices further calls for a denser network layout, which in turns partially shifts the focus to low- or medium power front-ends that can be mounted adjacent to, or even integrated with, the antenna. Thus, in order to avoid bulky and expensive cooling technology, it is of utmost importance that

the amount of dissipated power is minimized.

One very common method deployed to improve the use of the spectrum is Multiple-Input Multiple-Output (MIMO) systems which, as the name suggests, requires a dedicated RF front-end for each antenna in the array. This increasing number of transmitter chains stresses the importance of reducing both the physical and environmental footprint by means of optimizing the power efficiency. The cooling systems of today's transceivers, in particular for the RFPA, are one of the major contributors to the large footprint. Thus increasing the power efficiency of the system reduces not only the power dissipated into heat, but further decreases the need for bulky, active cooling technology and will therefore reduce the total footprint of each radio chain significantly.

Another need brought on by the mobile broadband evolution is the associated expansion of spectrum usage. This increases the need of flexible, reconfigurable solutions for future wireless network systems. Fig. 1.2a depicts a block-diagram of a traditional superheterodyne transmitter architecture which today is one of the most common topologies. The rapidly evolving computational capabilities in digital systems are today paving the road toward a possible Software Defined Radio (SDR) solution, [7, 8]. SDR has for quite some time been considered as a possibility to provide a highly flexible radio access technology platform. But one of the main obstacles that so far have hampered the development of a generic SDR system have been the lack of wideband RF technology with a wide frequency range providing an acceptable cost/performance trade-off. This means that there is a need for flexible systems that can adapt to new access technologies as well as providing frequency reconfigurability and possibilities to adapt output power without sacrificing efficiency. SDR systems with flexible RF front-ends are one way to meet these requirements. A block-diagram of a generic SDR transmitter is shown in Fig. 1.2b.

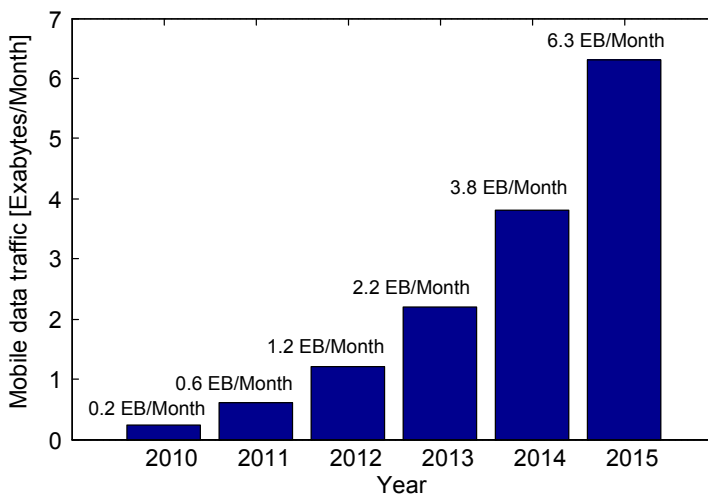


Figure 1.1: Forecast of global mobile data traffic over the period 2010-2015. Source: Cisco VNI Mobile, 2011, [3]

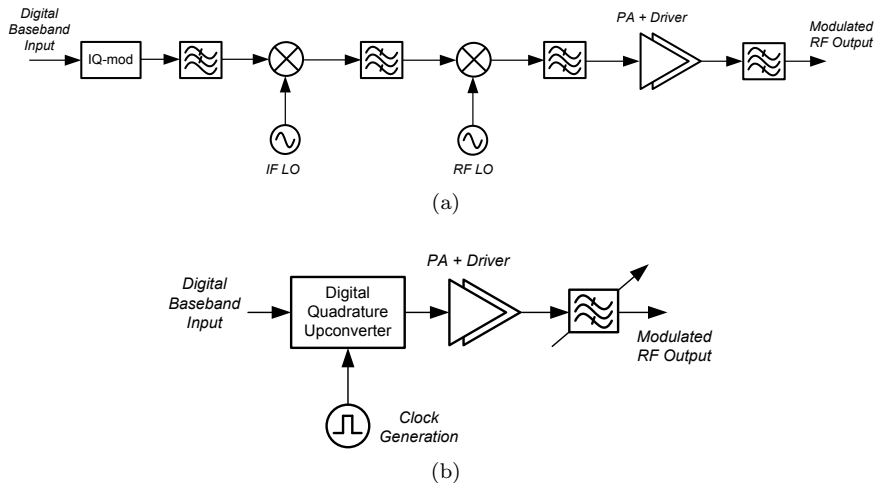


Figure 1.2: (a) Simplified sketch of a classical, superheterodyne RF transmitter. (b) Simplified sketch of an all-digital RF transmitter.

1.2 Thesis Contribution

The academic literature contains numerous methods designed for optimizing the power efficiency of the RFPA, a few of which is introduced in the following chapter. The pulsed RF transmitter, e.g. transmitters which utilizes a binary representation of the signal in conjunction with a Switched Mode PA (SMPA), have for quite some time been considered as a candidate for compact and highly integrated, high efficiency transmitters, [9]. However, there are still several issues regarding the implementation of such a transmitter that are hampering its development, some of which are addressed in this thesis.

The single-bit quantization schemes which are deployed in order to increase the RFPA efficiency, produces a vast amount of quantization noise. This noise needs to be removed by means of bandpass reconstruction filtering which, at microwave frequencies commonly suffers from large insertion loss if the fractional bandwidth is low. Paper I and II propose two methods which are both aimed at increasing the necessary reconstruction filter bandwidth, while keeping the pulse-rate at a moderate level, thus decreasing the insertion loss of the filter. The method can be used both separately, as well as jointly and are evaluated with promising results, using theoretical results, simulations and measurements.

Further on, Paper III examines the use of $\Sigma\Delta$ -modulation on general, complex-valued signals in two common domains - quadrature and polar. An issue commonly overlooked in the literature is identified and a solution is presented in the form of a complex $\Sigma\Delta$ -modulator. In a polar context, the proposed modulator further allows for coarse quantization of the phase-component, reducing the number of bits in total needed to achieve high signal fidelity.

Finally, the issue of concurrent multi-band operation is addressed in Paper IV-V, where an all-digital approach based upon quadrature low-pass $\Sigma\Delta$ -modulation is demonstrated.

1.3 Thesis outline

This thesis is organized as follows. First, the common power efficiency metrics is introduced in Chap. 2, followed by an overview of common efficiency enhancement techniques. Amongst the efficiency enhancement methods discussed in Chap. 2, the reader will find the so called pulsed RF transmitters in which different types of single-bit quantization schemes are deployed in order to improve the power efficiency of the transmitter. These quantization schemes are discussed in detail in Chap. 3, where the concept of Noise-Shaped Coding is introduced, with focus on the $\Sigma\Delta$ -modulator. Chap. 4 discusses the application of $\Sigma\Delta$ -modulation in a pulsed RF transmitter context. Finally, the thesis rounds of with some conclusions and notes on possible future work in the area.

Chapter 2

RF Power Amplifier Efficiency Enhancement Techniques

In this chapter, some of the most common RFPA efficiency enhancement techniques will be discussed. First, a brief introduction to the common efficiency metrics is given, followed by a treaty on the concept of dynamic supply modulation. This is followed by a section treating the three most common dynamic load modulation techniques - Doherty, Chireix outphasing and Varactor-based DLM (VDLM). Finally, an overview of the concept commonly referred to as pulsed or switched mode transmitter architecture is provided, which also serves as a background to the research presented in Chap. 4.

2.1 Efficiency Metrics

It should be well established by now that the power efficiency of the RFPA is an highly important parameter. However, before proceeding with further introduction of the power efficiency enhancement techniques commonly used in the RFPA field, we need to establish a measure of the RFPA performance in terms of power efficiency, or perhaps rather power conversion efficiency. In the literature, there are two figures of merit commonly associated with the RFPA power efficiency, which will be used here as well. These figures are commonly referred to as Drain Efficiency, commonly denoted as η , and Power Added Efficiency (P.A.E). Both of these figures are defined using the power relations shown in Fig. 2.1.

Drain Efficiency

The drain efficiency, or η , tells us the efficiency of the energy conversion, considering only the output circuitry of the RFPA. η is defined as the ratio between the delivered output power and the DC-power consumed by the RFPA,

$$\eta = \frac{P_{\text{out}}}{P_{\text{DC}}}. \quad (2.1)$$

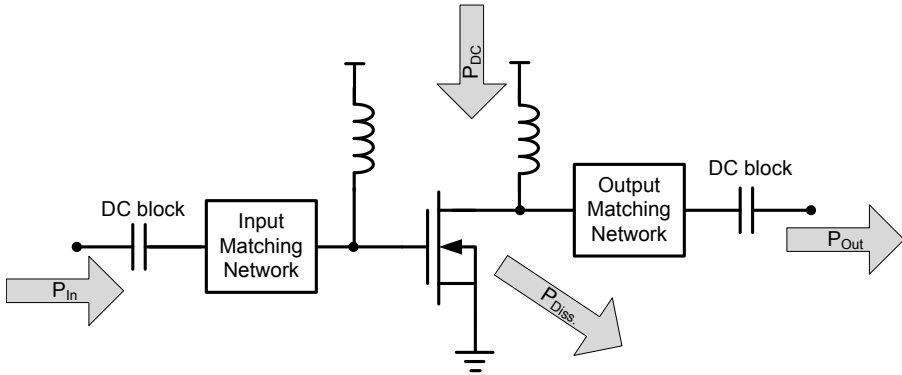


Figure 2.1: A simplified sketch an general RF Power Amplifier including input and output impedance matching networks. The arrows indicate the power relationships involved. The dissipated power, P_{diss} , transfers into heat and is lost, causing the efficiency to drop.

The specific term *drain efficiency* stems from the use of FET devices. For bi-polar type devices, the corresponding figure is commonly referred to as *collector efficiency*, but its definition does however stay the same.

Power Added Efficiency

For a more comprehensive understanding of the RFPA power conversion efficiency, we need to consider all the contributions to the process shown in Fig. 2.1. The figure of merit commonly referred to as P.A.E offers a more complete view of the power conversion than η , since it includes the necessary input drive signal power. PAE is defined as

$$\text{PAE} = \frac{P_{\text{out}} - P_{\text{in}}}{P_{\text{DC}}} = \eta \left(1 - \frac{1}{G} \right) \quad (2.2)$$

where G is the gain of the RFPA. It is clear from its definition that when $G \rightarrow \infty$, $\eta \rightarrow \text{PAE}$. One might then question the use of η since PAE provides a clearer view of the RFPA efficiency performance. However, much of the analysis related to RFPA efficiency is greatly simplified using η instead of PAE and will, provided enough gain, differ very little.

Now that the efficiency metrics are introduced, we will move on to discuss some of the common efficiency enhancement methods, starting with dynamic supply modulation.

2.2 Dynamic Supply Modulation

There are mainly two types of DSM techniques that are commonly treated in the literature. These are referred to as Envelope Elimination and Restoration (EER), [10], and Envelope Tracking (ET), [11]. The common ground of the two methods is that the drain bias voltage is modulated as a function of the signal envelope in order to reduce the dissipated power. The difference is mainly that

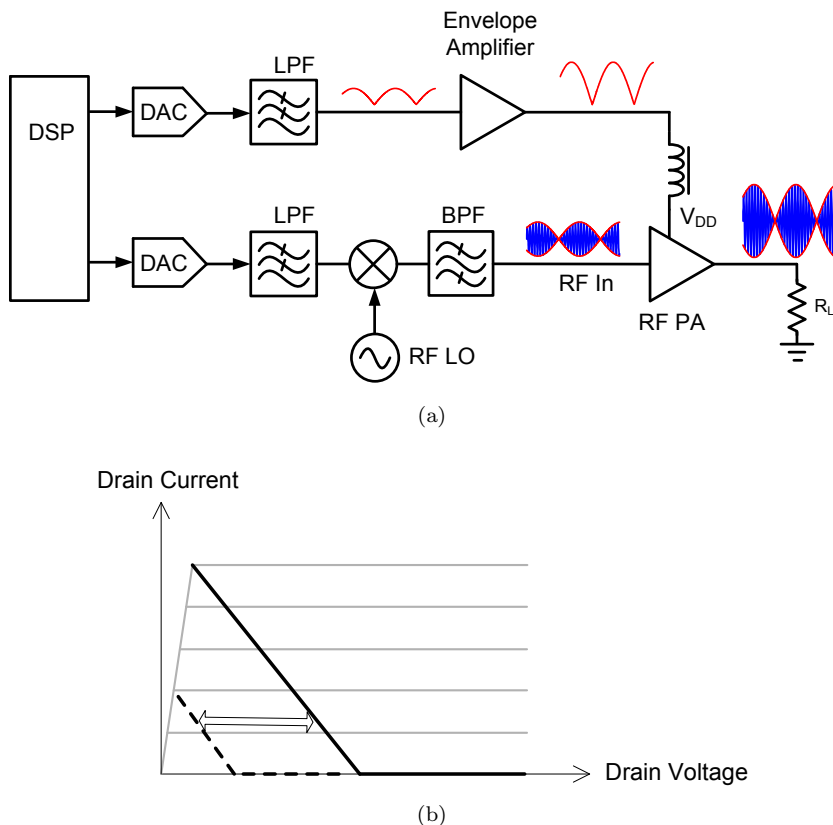


Figure 2.2: (a) A simplified block schematic of a typical envelope tracking system. (b) Intrinsic load-line trajectory of the RFPA for full and backed off output power during DSM operation.

for EER, the RFPA input consists of a constant envelope, phase-modulated RF carrier and the envelope of the output signal is controlled solely by the drain bias modulation. For ET, the drain bias modulation simply tracks the input signal envelope in order to minimize the dissipated power. A topological sketch of a EER/ET system is presented in Fig. 2.2a.

The dissipated power is minimized for backed off power operation by a horizontal shift of the load-line, as illustrated in Fig. 2.2b. This reduces the dissipated power by avoiding load-line trajectories in the high dissipation areas, which in turn increases the average efficiency.

Ideally, EER/ET schemes are capable of maintaining the RFPA peak efficiency independent of the output power. However, non-idealities in both the RFPA and the envelope amplifier, limits the performance of the system in several different ways. One issue often associated with EER/ET is the power efficiency of the envelope amplifier which, in combination with the bandwidth needed in order to exactly replicate the amplitude component. This tends to punish the envelope amplifier efficiency (η_{EA}) and reduce the overall system efficiency. The total efficiency can, in a simplified manner, be estimated as the product of the power efficiency of the envelope amplifier and the RFPA

respectively, as

$$\eta_{\text{Tot.}} = \eta_{\text{EA}} \cdot \eta_{\text{RFPA}} \quad (2.3)$$

where η_{RFPA} is the average RFPA drain efficiency. Thus, the efficiency gained on the RFPA side can potentially be lost in the envelope amplifier. Improvements can however be done by either improving the efficiency of the envelope amplifier, or deploy optimized bandwidth reduction schemes which trades off some efficiency in the RFPA in order to maximize $\eta_{\text{Tot.}}$. An empirical method for determining the optimal drain-voltage/input drive power relation is presented in [12].

Another important physical parameter which limits the performance of the EER/ET schemes, is the on-resistance of the transistor, R_{On} . The efficiency loss inflicted by R_{On} , [13], can be predicted by

$$\eta_0 = \frac{1}{1 + \gamma \frac{R_{\text{On}}}{R_L}} \quad (2.4)$$

in which γ is a constant depending on the intrinsic voltage and current waveform shapes. Here we see that the efficiency loss can be reduced by increasing the load impedance R_L . However, in order to maintain the output power, the drain-voltage needs to be increased, which puts additional stress on the envelope amplifier design. Since R_{On} also increases with maximum V_D , it is crucial to find a good trade-off in order to maximize the power efficiency of the total ET system.

Finally, in any polar scheme that treats amplitude and phase-components separately, the issue of synchronization arises. If the envelope-signal is not properly aligned with the RFPA input signal, unwanted distortion will arise as a product of the mismatch, [14]. The importance of synchronizing the two signal components increases with bandwidth as the spectral impact increases for a fixed time error as the signal bandwidth goes up.

2.3 Dynamic Load Modulation Techniques

This section will survey the concept of Dynamic Load Modulation (DLM) and three of the most common methods used for implementing DLM - The Doherty amplifier, the Chireix Outphasing amplifier and varactor-based DLM. The three different concepts have one thing in common, which is the fact that the load-impedance seen by the RFPA changes with the signal envelope, in order to improve the power efficiency.

A short overview of each concept is presented, followed by a short discussion on the advantages and disadvantages in each case. First in line is the Doherty amplifier, which will be followed by the Chireix outphasing amplifier and finally, the varactor-based DLM concept.

2.3.1 The Doherty Amplifier

The Doherty power amplifier, named after its inventor William H. Doherty who published the concept back in 1936, [15], has in recent days become one of the most popular efficiency enhancement methods. In its canonical form,

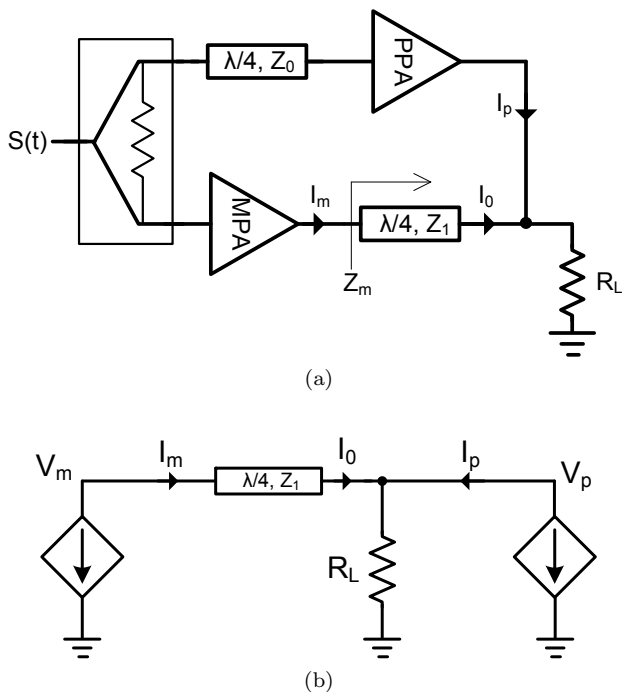


Figure 2.3: (a) A simplified topological sketch of a Doherty RFPA configuration, including a main (MPA) and a peak (PPA) amplifier. (b) A simple current source based model of the Doherty topology in (a).

it consists of two amplifiers and a combiner network, configured as illustrated in Fig. 2.3a. The two amplifiers are commonly referred to as main (MPA) and peak (PPA) amplifier, which indicates the output power range in which each stage works¹. Generalization of the Doherty concept for N amplifiers is possible and has been successfully demonstrated, [16], but for the sake of simplicity, only the $N = 2$ Doherty will be treated here.

The transition point, here denoted α , is defined as the normalized output voltage level at which the PPA starts conducting. Thus, it is assumed that the MPA is biased in class A/AB, while the PPA is operating in class C such that it only draws drain current for a normalized output voltage above the transition point α .

Now, in order to understand the load-modulation effect taking place in a Doherty amplifier, one needs to look closer at the output voltage and current for both the MPA and PPA, as depicted in the simplified current-source based model in Fig. 2.3b. V_m , I_m , V_p and I_p denotes the output voltages and currents from the MPA and PPA, respectively. Fig. 2.4a illustrates the ideal voltage/current relation for a classical, symmetrical Doherty setup, e.g. with $\alpha = 0.5$, [17]. The operation of the Doherty amplifier can be divided and described in the two regions - below and above α .

¹In some literature, the terms carrier and auxiliary are used instead of main and peak.

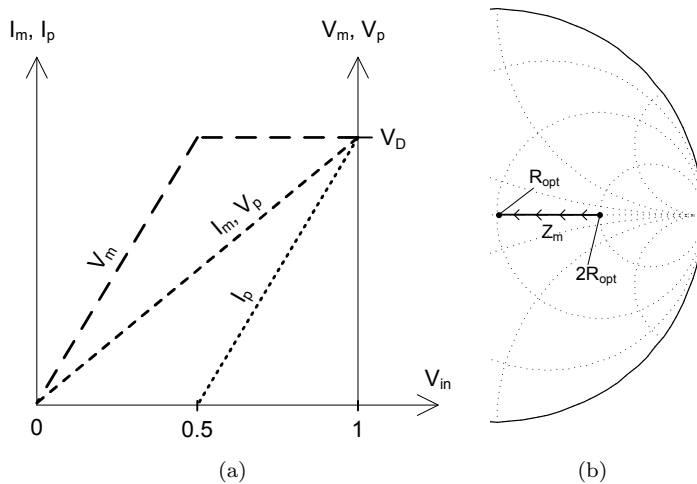


Figure 2.4: (a) The voltage-current relations of main and peak amplifier in an ideal, canonical Doherty amplifier. (b) Trajectory for Z_m as a function of input signal power. Arrows indicates increase in delivered output power.

Below α : During operation below the threshold, the impedance presented by the peak amplifier is ideally an open circuit. This allows the MPA to work as a regular class A/AB/B, single stage amplifier with fixed load-impedance, $2R_{opt}$.

Above α : After crossing the threshold, the PPA is put into operation at the same time as the drain voltage of the main amplifier, V_m , reaches its maximum. Due to the $\lambda/4$ transformer at the MPA output, the MPA output current, I_m , keeps increasing as a function of the PPA output current, I_p , as [17]

$$I_m = \frac{R_L}{Z_0} \left(\frac{V_m}{Z_0} + I_p \right). \quad (2.5)$$

where Z_0 is the characteristic impedance of the $\lambda/4$ transmission line. This creates a shift of the load-impedance seen by the MPA, Z_m , from $2R_{opt}$ to R_{opt} as illustrated in Fig. 2.4b. Finally, at peak output power, both amplifiers are working at R_{opt} and achieves peak efficiency.

A theoretical piecewise model of the Doherty RFPA efficiency, based upon the assumptions that two ideal class B power amplifiers are used, can be written as follows for the normalized case of $V_D = 1$, [18].

$$\eta = \begin{cases} \frac{\pi V_L}{4\alpha} & \text{if } 0 \leq V_L \leq \alpha, \\ \frac{\pi V_L^2}{4(V_L + \alpha(V_L - 1))} & \alpha < V_L \leq 1. \end{cases} \quad (2.6)$$

where V_L is the voltage over the load impedance, R_L . Simulated values for three different configurations of α , including the symmetric case of $\alpha = 0.5$, is presented in Fig. 2.5.

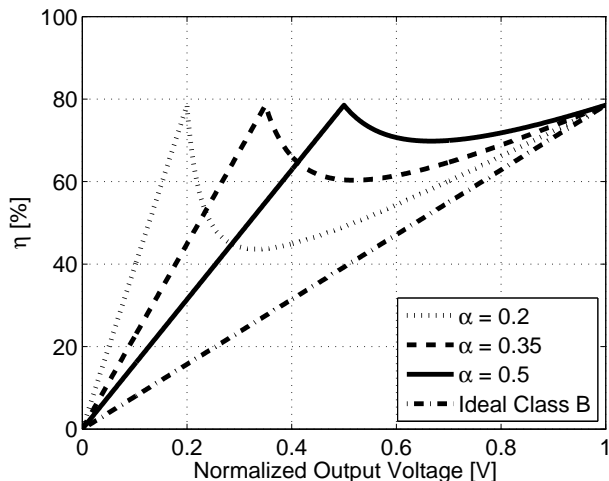


Figure 2.5: Resulting theoretical η for an ideal class B based Doherty RFPA for three different transition points, α .

Common issues related to the Doherty RFPA

There are several common issues related to the Doherty power amplifier that a practitioner of RFPA design needs to consider, many of which have been addressed in the academic literature during the last decade. The first, and fairly obvious issue is the bandwidth over which the Doherty amplifier correctly performs the load-modulation described in Fig. 2.4a and Fig. 2.4b. The limiting factor here is the $\lambda/4$ -transmission line which performs the impedance inversion. Combiners which enables concurrent dual band operation has been developed, [19], but the issue of instantaneous bandwidth resides.

Another limitation to the traditional (or so called analogue) Doherty concept, is the input power division which during the PPA off-state below α , wastes half of the power by feeding it to the inactive PPA. Several different approaches has been taken to battle this issue, for example a power-adaptive combiner, [20], and the so called digital Doherty, [21], in which the MPA and PPA are controlled separately.

2.3.2 The Chireix Outphasing Amplifier

The second DLM concept which, much like the Doherty amplifier, uses two power amplifier ... is the Chireix outphasing system. The concept of outphasing amplification, originally named “*Ampliphase*” by its original inventor H. Chireix, [22], is in theory a quite simple construct to understand. The Chireix outphasing configuration consists of two RFPAs whose outputs are combined via a combiner network, as for example the one illustrated in Fig. 2.6. It should be noted that, as in the Doherty case, the Chireix outphasing system can be generalized to a higher order, [23].

The operation of an outphasing amplifier is perhaps best illustrated using

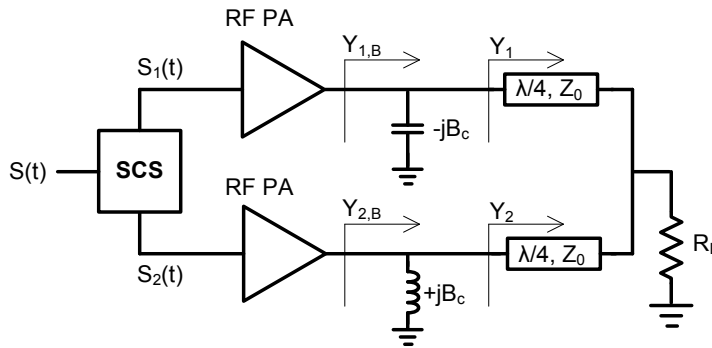


Figure 2.6: A simplified sketch of the Chireix outphasing system, including the $\lambda/4$ transmission-line based output power combiner, the SCS block and compensation reactances, $\pm jB_c$.

the product-sum rule. We can write the output signal $S(t)$ as

$$\begin{aligned} S(t) &= \frac{\hat{A}}{2} \cos(\omega t + \varphi(t) + \psi(t)) + \frac{\hat{A}}{2} \cos(\omega t + \varphi(t) - \psi(t)) \\ &= \hat{A} \cos(\psi(t)) \cos(\omega t + \varphi(t)) \end{aligned} \quad (2.7)$$

where \hat{A} is the total peak output amplitude and ψ is the outphasing angle. As we can see, the output amplitude is now controlled by means of the outphasing angle.

The normalized load impedance trajectory of each RFPA as a function of ψ , can be written as, [17],

$$\begin{aligned} Z_{1,B}(t) = Y_{1,B}^{-1}(t) &= \frac{1}{Y_1(t) - iB_c} = \frac{1}{\sin(\psi(t)) + i(\cos(\psi(t)) - B_c)} \\ Z_{2,B}(t) = Y_{2,B}^{-1}(t) &= \frac{1}{Y_2(t) + iB_c} = \frac{1}{\sin(\psi(t)) - i(\cos(\psi(t)) - B_c)} \end{aligned} \quad (2.8)$$

from which we now can observe that the ψ for which the RFPA load impedance becomes purely real, can be shifted by picking a different compensation reactance B_c , as illustrated in Fig. 2.7a. It should be noticed that the case for which $B_c = 0$ is commonly referred to as LINC, [24]. The resulting η have been derived and simplified for an ideal class B amplifier configuration, [17], and can be written as, [25],

$$\eta = \frac{\pi}{4} \cdot \frac{2 \sin^2 \psi}{\sqrt{(2 \sin^2 \psi)^2 + (\sin 2\psi - \sin 2\psi_c)^2}} \quad (2.9)$$

where $B_c = \sin 2\psi_c$ for a normalized $R_L = 1$. Thus, knowing the input signal statistics it is possible to optimize the average efficiency of the Chireix outphasing system by selection of the compensation reactance, B_c .

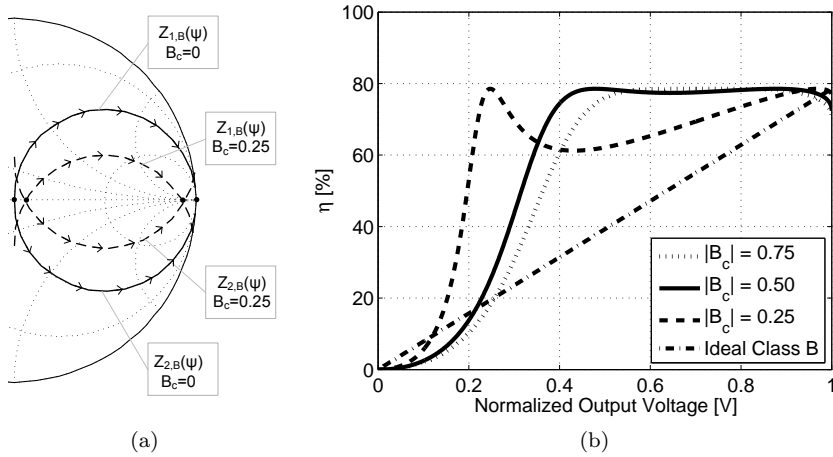


Figure 2.7: (a) Trajectories for $Z_{1,x}$ and $Z_{2,x}$ as a function of ψ for $B_c = 0$ and for $B_c = 0.25$. Arrows indicate the progression of ψ and dots mark the state in which both amplifiers see a purely resistive load, which results in the second efficiency peak. (b) Resulting theoretical efficiency for an ideal class B based Chireix outphasing system for three different, normalized compensation reactances, $|B_c|$.

Common issues related to the Chireix outphasing system

One way to view the concept of outphasing, is as the addition of two vectors, where the magnitude of the resulting vector $S(t)$ is a function of the outphasing angle $\psi(t)$ between the constant-magnitude vectors $S_1(t)$ and $S_2(t)$. This way of viewing it reveals one of the major drawbacks with "pure" outphasing amplification, which is that in order to represent zero output power, still requires two RFPAs working at full output power. Another issue which arises is that the impedance trajectories applied to each RFA are taking two different directions, e.g. one RFA will see an increasingly capacitive load while the other will see an increasingly inductive load. A remedy to both of these issues is to apply an (possibly asymmetric) amplitude control for the low power region, as presented in [o], [26], which will increase the overall PAE while maintaining the efficiency increase achieved at medium to high power operation.

2.3.3 Varactor-based Dynamic Load Modulation

We have now arrived to the final method of implementing DLM covered in this section, namely the varactor-based DLM scheme. Here, the load-modulation of the RFA is performed using an electrically tunable matching network, as illustrated in Fig. 2.8a, which allows for dynamical load impedance adjustments of the amplifier. The tunable network is most commonly based on varactor diodes, [f], but other approaches has been suggested, such as utilizing the non-linear, voltage dependent output capacitance of a MOSFET-device, [27]. Two different design approaches are presented in [28], which provides intuitive

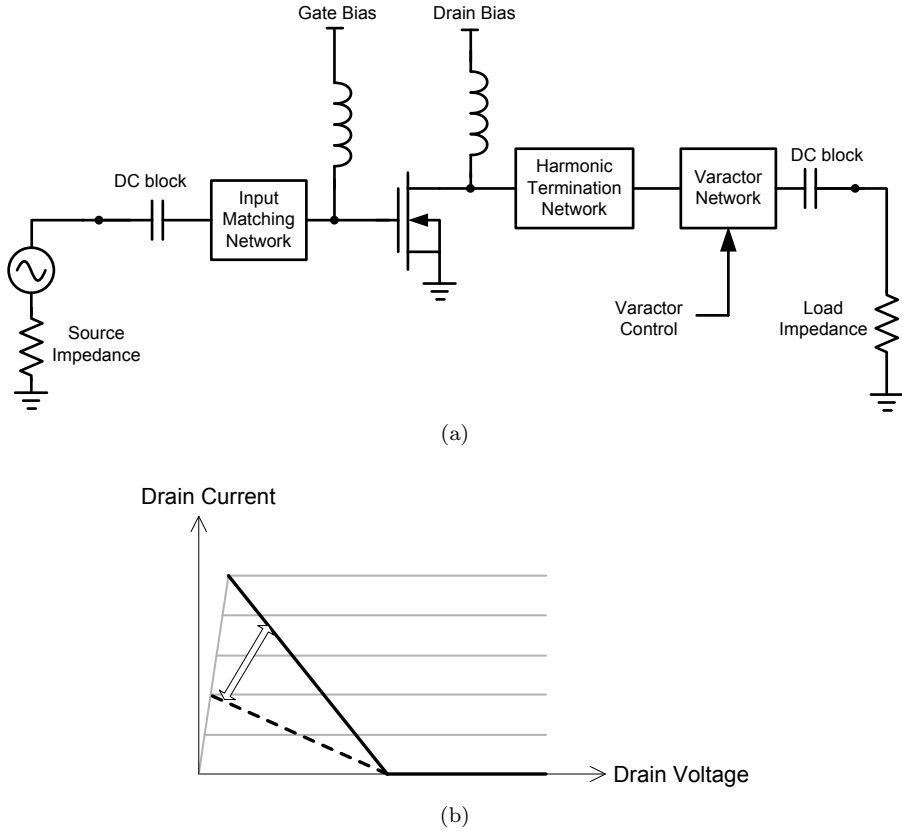


Figure 2.8: (a) A simplified sketch of a VDLM architecture. (b) The load-line trajectory under ideal DLM operation.

tools for designing both the varactor network and RFPA, either separately in a modular approach, or jointly.

The potential gain in terms of power efficiency associated with VDLM are very large, in fact - theoretically, the RFPA should be able to maintain peak efficiency over the whole range of output power. However, loss-mechanisms in both the varactor-based network as well as the RFPA limits the performance to some extent, but a large portion of efficiency gain still resides. Fig. 2.9 shows simulations performed on a LDMOS-based class F^{-1} amplifier at 1 GHz, which illustrates the potential efficiency increase provided by the VDLM-technique. As shown, both the input signal drive as well as the varactor capacitance are swept and the efficiency characteristics achieved by the optimal signal power/varactor capacitance is highlighted. The VDLM concept has been demonstrated both for low- to medium power-levels below 1 W, [29,30], as well as for power levels as high as 10 W peak output power, [h], [31].

Common issues related to VDLM RFPA's

As discussed in [k], one of two major issues related to the VDLM technique is the breakdown voltage of the varactors used, the second being C-V charac-

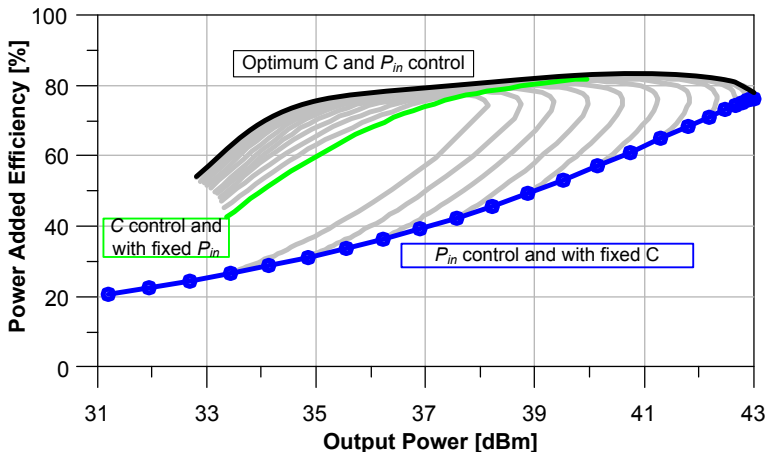


Figure 2.9: Simulated PAE of a class F^{-1} LDMOS amplifier working at 1 GHz using an ideal varactor as presented in [q].

teristics of the varactors. In [m], a SiC varactor with customized C-V characteristics and high breakdown voltage is presented. Another issue related to VDLM-network is the nonlinear distortion inflicted by the VDLM-network. The linearity performance of the VDLM can however be improved by the use of anti-serial varactor stacks, [32], or by use of digital pre-distortion linearization schemes, [33].

As stated in the previous section, the VDLM concept can in theory, unlike the Doherty and Chireix concepts, keep the load-impedance optimized over a large range of output power. However, scaling in terms of increasing the peak output power has so far not reached the same level as that of the multi-transistor concepts such as the Doherty and Chireix.

Finally, due to the added degree of freedom provided with a second envelope control input, a need for an efficiency and linearity optimized dual-input control scheme is called for, as well as a method for synchronizing the two different inputs. Most of these issues related to VDLM, have been addressed and methods for dealing with both efficiency and linearity have been developed, [33–35].

Extending the Doherty/Chireix techniques by VDLM.

It should be noted that the three different implementations of DLM presented in this chapter are by no means incompatible with each other, and can in fact be combined. One example of this is shown in [p], where it is described in detail how varactor networks can be used in order to dynamically tune critical design parameters and increase the overall efficiency of both Doherty and Chireix configurations.

In the Doherty case, the varactor network is set up to dynamically adjust the characteristic impedance of the impedance inverting $\lambda/4$ transmission line. This effectively moves the transition point α , which as described in section 2.3.1 can dynamically shift the efficiency peak to a desired location. In the Chireix

case, the VDLM network can be configured in order to tune the compensation reactance B_c , which then can provide a purely resistive load to the RFPA, keeping the power efficiency high over a larger range of output power.

2.4 Pulsed RF Transmitter Architectures

The idea of high efficiency pulsed or switched mode operation stems from the area of RPM-control in electrical AC-engines, [36, 37]. It later found its way into the area of audio amplification, where it has been successfully used since the late 1960s. One of the earliest recorded use of PWM in audio amplification was filed in as a patent by J. Gregory, [38], already in -66. In the last couple of decades, switched mode operation has found its way into high efficiency DC/DC-converters along with the development of SiC FET and GaN HEMT technology.

The fundamental idea of pulsed mode operation is to use the transistor as a switch, operating only in two states - full output power or completely off. It is in these two states that the amplifier works efficient in terms of power conversion. The pulsed RF transmitters can be divided in two major categories depending on what level the single-bit quantization is performed - RF or baseband. Here follows a brief description of the two categories, including some examples of architectures for each category.

2.4.1 RF-level Pulsed Transmitter Architectures

RF-level pulsed transmitters architectures can be described as a transmitter which relies on a full digital, direct to RF type of single-bit quantization scheme, which produces a single-bit representation of the modulated RF signal. This single-bit representation is then fed to a high efficiency RFPA before reconstructing the signal by means of linear filtering. These architectures are commonly strongly associated with, and considered good candidates for a fully digital RF transmitter. A simplified block-schematic of a general RF-level pulsed-transmitter architecture is shown in Fig. 2.10.

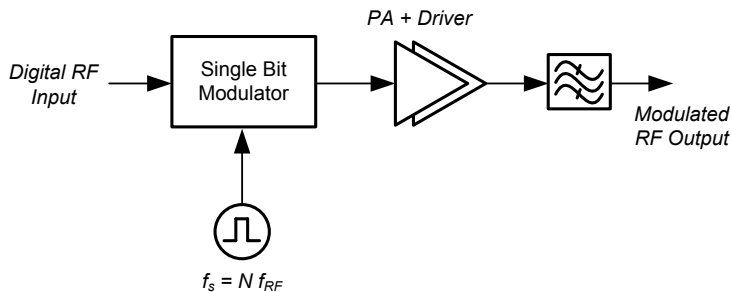


Figure 2.10: A principal sketch of a general RF-level pulsed transmitter architecture where the sample-rate of the modulator commonly has an integer relation to the RF carrier frequency, $f_s = N f_{RF}$, where $N > 1$ usually is an integer.

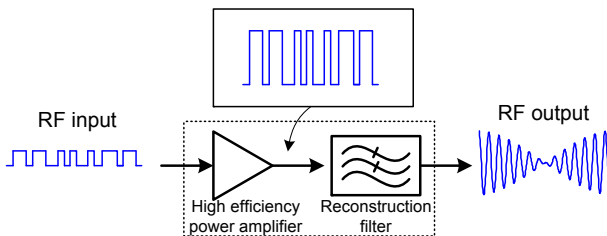


Figure 2.11: A highly simplified illustration of a RF-PWM transmitter. The RFPA is fed a pulse-train at a rate related to the RF carrier frequency which, after amplification is reconstructed by means of filtering.

There are two very common types of architectures occurring in the academic literature, both named after the type of single-bit modulation scheme involved in the process: the RF bandpass $\Sigma\Delta$ - and RF PWM-modulators.

First, the RF Bandpass $\Sigma\Delta$ -modulator based transmitters, [39–48], in which a bandpass $\Sigma\Delta$ -modulator is deployed in order to directly create a binary representation of the modulated RF carrier. The signal then needs to be recovered by means of a bandpass reconstruction filter, before delivered to the load.

The second approach is the RF-PWM, [49–52], which is a scheme where the amplitude and phase of the modulated RF carrier is encoded using PWM/PPM. A simplified sketch of RF-level pulsed operation of an RFPA is illustrated in Fig. 2.11. For the case of PWM, the process of reconstruction filtering can be simplified provided that the granularity of the pulse-width and position is fine enough. Ideally, the only component in a PWM scheme which needs filtering will then be the odd harmonics of the pulse-rate, which is located far from the carrier and needs simply a low-pass filter.

It should be noted that the RF level transmitter architectures require either a very large sample rate, commonly an integer multiplier of the RF carrier frequency, or an analogue or continuous-time system which commonly requires a feedback loop, [52]. Both approaches come with related advantages and disadvantages however. The advantage of the analogue approach is commonly reduced power consumption due to the lack of high frequency clock. However, for very large signal bandwidths, the stability of an analogue feedback-based approach might suffer due to the need for a large loop-bandwidth, [53].

2.4.2 Baseband-level Pulsed Transmitter Architectures

Another class of pulsed RF transmitter architectures, are the ones which incorporate the single-bit quantization scheme on a baseband level, before performing some sort of upconversion of the baseband signal onto a RF carrier. This can be accomplished in either analogue or digital domain by means of a mixer, [54, 55], as illustrated in Fig. 2.13a, or by means of a Digital Up-Converter (DUC), [56], as illustrated in Fig. 2.13b. In [56], the DUC consists of three high-speed multiplexers (MUX) which not only performs the upconversion, but also combines the $\Sigma\Delta$ -modulated quadrature components of the signal. Other such methods would include a Digitally Controlled Os-

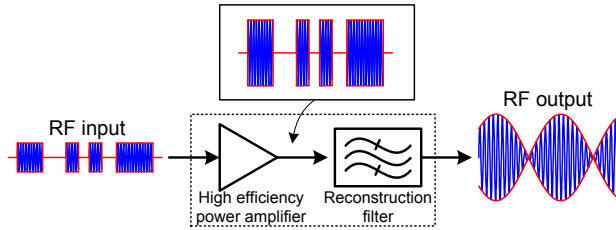


Figure 2.12: A highly simplified illustration of a baseband-level pulsed RF transmitter.

cillator (DCO [57]), for example [58] or an All-Digital Phase-Locked Loop (ADPLL), [59]. A simplified sketch of baseband-level pulsed RFPA operation is illustrated in Fig. 2.12.

In both approaches, the pulse-rate of the $\Sigma\Delta$ -modulator is proportional to an integer multiple of the baseband signal bandwidth, as indicated in Fig. 2.13a where f_{BB} is the baseband sample rate and $N_0 \geq 1$ is an integer. This simplifies matters of implementing such a scheme due to the low modulator sample-rate, switch-losses e.t.c. However, as indicated in Fig. 2.13b where f_{RF} is the carrier frequency and $N_1 \geq 1$ is an integer, the fully digital approach requires a very large sample-rate.

The group of baseband-level pulsed transmitter architectures is usually divided into two different subgroups, depending on which coordinate system that is used to describe the signal space. The details of these two groups will be treated further in Chap. 4.

Common issues related to pulsed RF transmitters

As in the case of DSM and DLM, there are of course a few known fundamental issues related to the pulsed RF transmitters, some of which will be addressed in Chap. 4. The first and most obvious issue is that of reconstructing the signal in terms of removing the large amount of quantization noise inflicted by the single-bit modulator. Narrowband filters at microwave filters are known to have a large insertion loss, [60], which leads to power dissipation and thus, reduced power efficiency. Another somewhat related issue is that of the required pulse-rate needed to provide good enough, post-reconstruction, signal fidelity. Increased pulse-rate leads to improved signal fidelity and the possibility to use wideband reconstruction filters with lower insertion loss, but causes increased power dissipation due to switch-losses in the RFPA.

2.5 Discussion

This chapter has provided a brief overview of the three most common RFPA efficiency enhancement methods - DSM, DLM and pulsed RF transmitters. Methods deploying different types of DSM or DLM, such as ET and the Doherty amplifier, are today considered a commodity. Pulsed transmitters however, are still facing some major challenges which need to be overcome in order

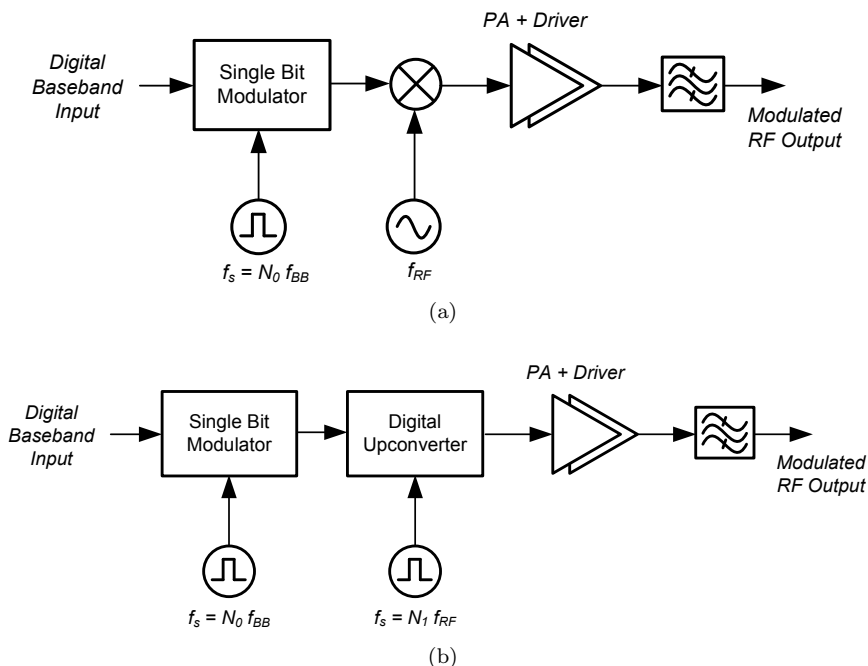


Figure 2.13: Highly simplified block-diagrams of baseband-level pulsed transmitter architecture using (a) analogue upconversion using a mixer and (b) digital upconversion. In both cases, the sample-rate of the modulator commonly has an integer relation, N_0 , to the baseband sample-rate, f_{BB} . For the digital upconversion in (b), the digital upconverter does however require a sample-rate at an integer multiple, N_1 , that of the carrier frequency, f_{RF} .

to provide high efficiency and ideally a fully digital RF transmitter implementation.

We will now move on to treat the concept of Noise-Shaped Coding in Chap. 3, which is a central part of most pulsed RF transmitters. Focus will be placed on the $\Sigma\Delta$ -modulator, being by far the most common technology for NSC. We will further discuss and analyze both common as well as novel methods for $\Sigma\Delta$ -modulator design and the possibilities these can provide for a pulsed RF transmitter. After this treaty on Noise-Shaped Coding, we will in Chap. 4 return to discuss $\Sigma\Delta$ -modulation based, pulsed RF transmitters in a more detailed fashion than the overview provided in this chapter.

Chapter 3

Noise-Shaped Coding

This chapter examines a single-bit quantization scheme commonly deployed for pulsed RF transmitter architectures in order to increase the RF power amplifier efficiency at the same time as keeping the signal fidelity high. The chapter introduces the concept of Noise-Shaped Coding and the most common method of implementing NSC, namely the $\Sigma\Delta$ -modulator. First, section 3.1 illustrates the concept of NSC by means of a simple, theoretical example in which a constant DC-level is encoded and analyzed. Section 3.2 introduces the $\Sigma\Delta$ -modulator and reviews common design methods.

3.1 A definition of Noise-Shaped Coding

The term *Noise-Shaped Coding* (NSC), as coined by Schreier in [61], refers to a quantization-scheme in which the spectral shape of the resulting quantization noise¹ is optimized in order to minimize a weighted quantization error metric. One example of such metric is the residual quantization error power after applying a linear filter on the quantized signal, which is the metric used throughout this thesis. Before moving on to investigate the use of NSC as an efficiency enhancement scheme in pulsed RF transmitter architectures, and in particular the use of so called $\Sigma\Delta$ -modulation, a clarification of the NSC concept is needed. This is here done by means of a simple, theoretical example.

NSC exemplified

Consider a sequence of 16 noise-free samples taken from a DC source, $x = \frac{1}{2}$. We will denote this sequence as

$$x = \underbrace{\left[\frac{1}{2}, \dots, \frac{1}{2} \right]}_{16 \text{ samples}}. \quad (3.1)$$

¹The term *quantization noise* stems from the noise-like behavior of the quantization error.

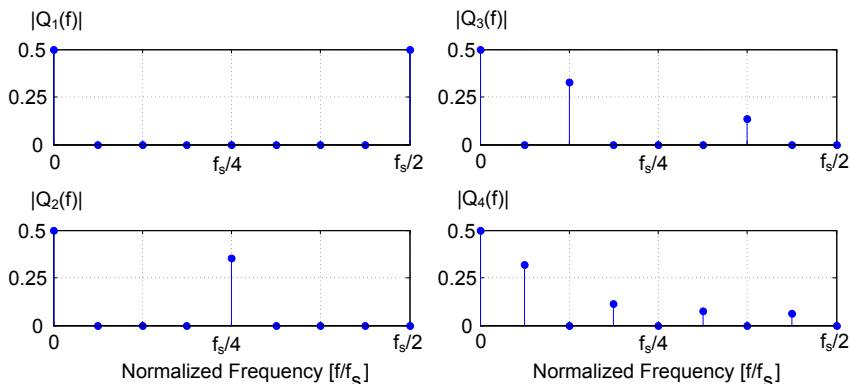


Figure 3.1: Calculated magnitude spectrum, $|Q_n(f)|$, of the quantization schemes presented in (3.2).

Now, we wish to quantize x using the values $\{0, 1\}$, which then will yield a quantized sequence $q_n \in \{0, 1\}^{16}$. The three cases we will consider here are

$$\begin{aligned}
 q_1 &= [1, 0, 1, 0, 1, 0, 1, 0, 1, 0, 1, 0, 1, 0, 1, 0] \\
 q_2 &= [1, 1, 0, 0, 1, 1, 0, 0, 1, 1, 0, 0, 1, 1, 0, 0] \\
 q_3 &= [1, 1, 1, 1, 0, 0, 0, 0, 1, 1, 1, 1, 0, 0, 0, 0] \\
 q_4 &= [1, 1, 1, 1, 1, 1, 1, 1, 0, 0, 0, 0, 0, 0, 0, 0]. \quad (3.2)
 \end{aligned}$$

The power spectral density (PSD) of each quantized sequence is presented in Fig. 3.1, from which we now can make a few observations.

1. The DC-component is exactly represented in all three schemes and can be perfectly recovered by means of linear low-pass filtering, such as

$$q_n \circledast f = x \quad (3.3)$$

where f is the impulse-response of a linear filter and \circledast is the convolution operator.

2. The PSD of the quantization error, or the *Noise Shape*, differs in each quantization of X . Thus, we say that (3.2) constitutes three different NSC versions of x .

This example clearly illustrates how an oversampled single-bit quantization and a linear reconstruction filter, makes it possible to create the resolution of a multi-bit quantization by means of one single bit. Thus, by carefully select the single-bit quantization scheme, a bulk of the quantization noise can be migrated to the stop-band frequencies of a supposed reconstruction filter.

Modulation by pulse width, position and density

There are two very common methods for creating an oversampled single-bit representation of a signal which, as illustrated above, will yield the original

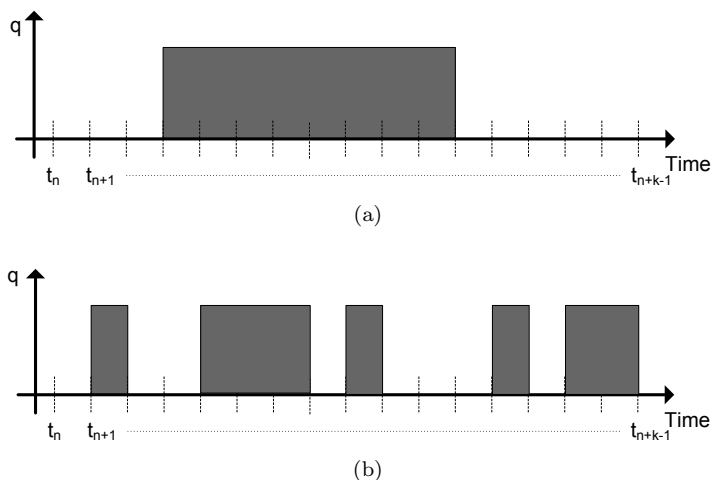


Figure 3.2: (a) An illustration of PWM/PPM with granularity $1/k$. Over the interval $[n, n + k - 1]$, one pulse with a width proportional to the input signal magnitude, gets placed at a position according to the phase of the input signal. (b) An illustration of PDM in which a pattern of pulses are distributed within the interval $[n, n + k - 1]$ according to the amplitude and phase of the input signal.

signal after linear reconstruction filtering. These encoding schemes map certain characteristics of the signal on to some corresponding characteristic of a binary pulse-train according to a set of rules. These mappings are commonly sorted into one of the following two groups.

- **Pulse Width and/or Position Modulation (PWM/PPM)**

The amplitude and phase information of the signal is encoded by modulating the width and position of the pulses respectively, as depicted in Fig. 3.2a.

- **Pulse Density Modulation (PDM)**

The amplitude and phase information of the signal is encoded in the distribution of fixed-duration pulses, as exemplified in Fig. 3.2b.

The minimum pulse-duration is, in both cases, determined by the oversampling ratio (OSR) of the signal.

As illustrated in Fig. 3.2, PDM adds a degree of freedom in terms of pulse placement which is needed in order to improve the SQNR by means of NSC. However, for applications in which each pulse-transition adds to the power dissipation by means of switching losses, such as DC/DC conversion or pulsed RF transmitters, the PWM/PPM is sparse in terms of transitions in comparison with PDM, as illustrated in the theoretical example. However, for a given minimal pulse-length, the PDM schemes will improve the signal fidelity compared to PWM/PPM. The frequency spectrum of the quantization noise generated by PWM has been exactly analyzed, [62, 63].

In an audio context, NSC is commonly deployed in dithering-based bit-reduction schemes. Here, a dithering signal, which is commonly white noise,

is applied in order to increase the effective bit-resolution of the encoded signal. The NSC scheme then shapes the spectrum of the dithering-signal and concentrates most of its energy to parts of the spectrum for which the human ear, which here also acts as a reconstruction filter, is less sensitive, [64]. Similar methods are well developed for use in video-coding, [65], in which the quantization error of each pixel, is diffused onto the neighboring pixels, thus making the coarse, low resolution quantization harder to detect by the human eye which, just as the ear, acts as a reconstruction filter.

A different approach to NSC which gives a maximum likelihood sequence: [66–68].

In the remainder of this chapter, the focus will lie on PDM due to its strong connection with $\Sigma\Delta$ -modulators. With these results in mind, we will now move on to discuss the topic of $\Sigma\Delta$ -modulation, which is by far the most common method used for NSC.

3.2 Noise-Shaped Coding by $\Sigma\Delta$ -Modulation

The $\Sigma\Delta$ -modulator, [69–71], is a class of oversampled A/D converters, originally invented in the 1950's [72, 73]. Over the course of the years since its invention, the $\Sigma\Delta$ -modulator has gained huge popularity. One significant advantages of using oversampled, single-bit converters as the $\Sigma\Delta$ -modulator is the built-in invariance to circuit variations due to the feedback topology, as well as improved linearity in comparison to regular Nyquist-rate, multi-bit quantization schemes, [71].

In its canonical form, as illustrated in its 1st and 2nd in Fig. 3.3, the $\Sigma\Delta$ -modulator consists of a quantizer embedded within a feedback loop in which an integrator is introduced in order to shape the spectrum of the resulting quantization error as described in section 3.1. This topology was the result of an extension of the so called Δ -modulator, [74], in which the reconstruction filter - the integrator, has been included in the feedback loop, thus the added Σ . The single-loop modulator shown in Fig. 3.3a have been thoroughly analyzed by Gray et. al., [75–78].

In this thesis, the focus will lie on single-bit quantizer based $\Sigma\Delta$ -modulation, but it should however be noticed that most of the results can be generalized for use with a multi-bit quantizer.

3.3 Design and Analysis of $\Sigma\Delta$ -modulators

There is a vast base of both books and published research papers on the topic of $\Sigma\Delta$ -modulation and NSC. However, the state of the theoretical analysis have for a long time been lagging behind the empirical and practical research on the topic. This section will provide a short overview of some common tools used for design and analysis of $\Sigma\Delta$ -modulators.

3.3.1 The Linear Noise Model

Due to the nonlinear behavior of the $\Sigma\Delta$ -modulator, deterministic analysis of the spectral properties of the quantization error can be rather tedious and

sometimes, even impossible, in particular for high order modulators. Formal spectral analysis of specific $\Sigma\Delta$ -modulator structures have been performed, but the results are usually mathematically tedious and difficult to utilize for a $\Sigma\Delta$ -modulator designer, [79].

Therefore, a common method used for designing the loop-filters is to linearize the system by replacing the nonlinear quantizer function by a linear, additive noise-source. This provides the opportunity of using well established, classical linear systems analysis methods both for designing the modulator as well as prediction of SQNR and stability.

The Pseudo Quantization Noise Approximation

The quantizer PQN-approximation is a very common linearization technique used for analysis of the quantization noise spectrum in $\Sigma\Delta$ -modulators, [69–71, 80]. The linear noise-approximation of the error produced in a quantization process is valid under certain conditions defined by Bennett, [81], and later refined by Sripad and Snyder, [82]. It is however very common, in particular for the single-bit quantizer case, that none of the conditions specified in [81, 82] are fulfilled, which makes the validity of the PQN approximation rather questionable. Despite all this, it is still the most commonly used tool for analyzing the quantization noise spectrum of a $\Sigma\Delta$ -modulator.

The quantized output, $q[n]$, of a quantizer with input $x[n]$ can now be described as

$$q[n] = x[n] + e[n] \quad (3.4)$$

where e is a random variable uniformly distributed within $[-\Delta/2, \Delta/2]$ with white power spectrum and Δ is the quantizer step-size. Given the input signal distribution and the quantizer function, we can easily calculate the total quantization noise power. The average quantization noise power of a scalar

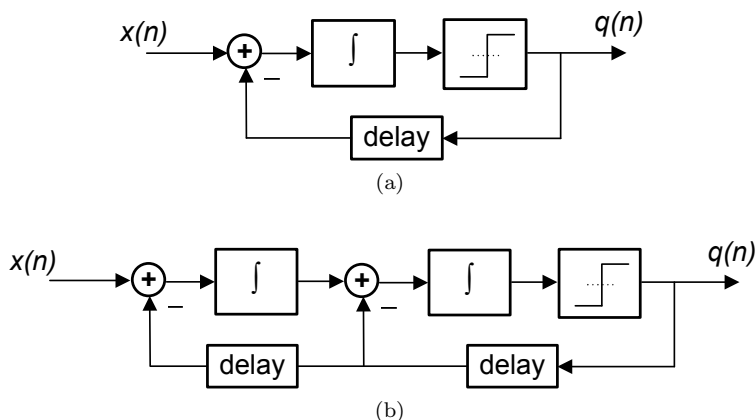


Figure 3.3: The canonical (a) first order and (b) second order integrator based low-pass $\Sigma\Delta$ -modulator.

quantizer, [83], can be calculated as

$$\sigma_e^2 = \mathbb{E} [|x - q|^2] = \sum_{k=0}^K \int_{T_k} |x - q_k|^2 p_x(x) dx \quad (3.5)$$

where p_x is the PDF of the input signal x and q_k is the reproduction point associated with the cell T_k . Using this PQN-model, we can now assemble a linearized modulator noise model.

Signal- and Noise Transfer Functions

The described linearization of the quantizer leads to a dual input, single output model which is shown for a general modulator topology in Fig. 3.4, where $X(z)$ is the reference signal input, $E(z)$ is the additive quantization noise, $H(z)$ and $G(z)$ are the loop-filters and $Y(z)$ is the resulting output signal as described in frequency domain. The linearized approach makes it possible to break the feedback loop and describe the system in terms of two transfer functions - one for the signal (STF) and one for the noise (NTF), [84]. Starting from the left of the modulator in Fig. 3.4, we know that the STF is defined as the transfer function from $X(z)$ to $Y(z)$, provided that $E(z)$ is kept zero. Thus, the STF can be calculated as

$$\text{STF}(z) = \left. \frac{Q(z)}{X(z)} \right|_{E(z)=0} = \frac{H(z)}{1 + z^{-1}H(z)G(z)} \quad (3.6)$$

while the NTF is defined as the analogue of the above, but with the input $X(z)$ being kept zero, which results in

$$\text{NTF}(z) = \left. \frac{Q(z)}{E(z)} \right|_{X(z)=0} = \frac{1}{1 + z^{-1}H(z)G(z)} \quad (3.7)$$

It is now possible to simply insert the coefficients for $H(z)$ and $G(z)$ in order to get a view of the quantization noise shape and to estimate performance in terms of SQNR.

In order to illustrate the gain of increasing the order of the NTF, we can study the N :th order generalization of the canonical low-pass modulator, [71],

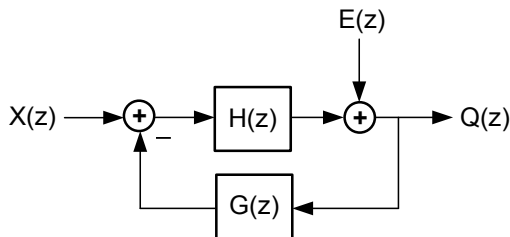


Figure 3.4: A general linearized model of a $\Sigma\Delta$ -modulator with loop-filters $H(z)$ and $G(z)$.

which produces the NTF

$$H(z) = \frac{1}{(1 - z^{-1})^N} \quad (3.8)$$

$$G(z) = z^{-1}. \quad (3.9)$$

Using (3.7) and replacing $z = e^{i\omega}$, we get the N :th order NTF as

$$\text{NTF}(\omega) = (1 - e^{i\omega})^N \quad (3.10)$$

with has the squared magnitude

$$|\text{NTF}(\omega)|^2 = \left[2 \sin\left(\frac{\omega}{2}\right) \right]^{2N}. \quad (3.11)$$

Now, using the PQN-approximation in (3.4), we can calculate the PSD of the modulated output using the STF/NTF-based linear model. This is simply written as a dual-input filter of two independent, random variables

$$\Phi_q(\omega) = \Phi_x(\omega) |\text{STF}(\omega)|^2 + \sigma_e^2 |\text{NTF}(\omega)|^2. \quad (3.12)$$

Due to the use of oversampling, the $\Sigma\Delta$ -modulator will appear transparent in the signal path, i.e. that $\Phi_x(\omega) |\text{STF}(\omega)|^2 = \Phi_x(\omega)$ in the PQN-model. This enables a further simplification of (3.12) as

$$\Phi_q(\omega) = \Phi_x(\omega) + \sigma_e^2 |\text{NTF}(\omega)|^2. \quad (3.13)$$

The positive impact of the increased NTF order in terms of SQNR is now clearly visible when studying the quantization noise spectrum. Fig. 3.5 shows the derived NTFs for both the 1st and 2nd order low-pass modulators, in comparison with the white noise term σ_e^2 .

Optimization based $\Sigma\Delta$ -modulator design

Due to the linearization described in the previous system, it is possible to use regular, linear optimization techniques in order to synthesize a NTF, from which loop-filter coefficients can be selected. Well defined methods exists for fitting a filter against constraints on its magnitude response, [85]. Commercially available toolboxes has been developed around this, [86], which were used for benchmarking in Paper I.

3.3.2 Stability Analysis

One very difficult issue of highly nonlinear feedback systems such as the $\Sigma\Delta$ -modulator, is stability. It was in fact commonly believed, until 1987, that single-bit $\Sigma\Delta$ -modulators with loop-filters of greater order than 2 was impossible to stabilize, [87]. However, since then, methods for characterizing the stability of the modulator have been developed, along side with methods for stabilization. This section reviews some common methods for performing stability analysis for a given $\Sigma\Delta$ -modulator.

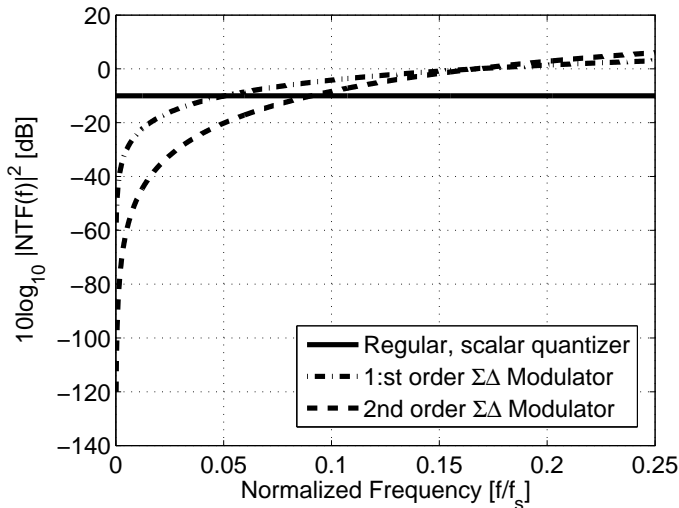


Figure 3.5: Theoretical NTF for 1st and 2nd order low-pass $\Sigma\Delta$ -modulators, in comparison with the regular scalar quantizer with white quantization noise power spectrum.

The Lee Criteria

Based upon the linearized modulator approach in which the quantizer is replaced with a PQN approximation, a method for predicting a priori stability have been suggested by Lee et. al., [88]. This criteria is commonly referred to by the name of its inventor and states that a modulator is likely to be stable if

$$\|\text{NTF}(\omega)\|_{\infty} < 1.5. \quad (3.14)$$

The Lee criteria is commonly used as a constraint in the linear optimization methods mentioned in the previous section. This approach to a priori stability predictions is however a bit suspicious and should be used with extreme care and complimentary, extensive simulations, [71]. This since it uses a linear approximation in order to determine stability behavior of a highly nonlinear system.

Input-to-State Stability

Using a state-space representation of a modulator, stability can be examined from the behavior of the internal states. Lets consider the state-space equation for the 2nd order $\Sigma\Delta$ -modulator depicted in Fig. 3.6a. Bounds for the internal state variables, r_1 and r_2 , under a constant input signal, have been derived by Zakhor et. al., [89], as

$$\|r_1\|_{\infty} \leq |x| + 2 \quad (3.15)$$

$$\|r_2\|_{\infty} \leq \frac{(5 - |x|)^2}{8(1 - |x|)}. \quad (3.16)$$

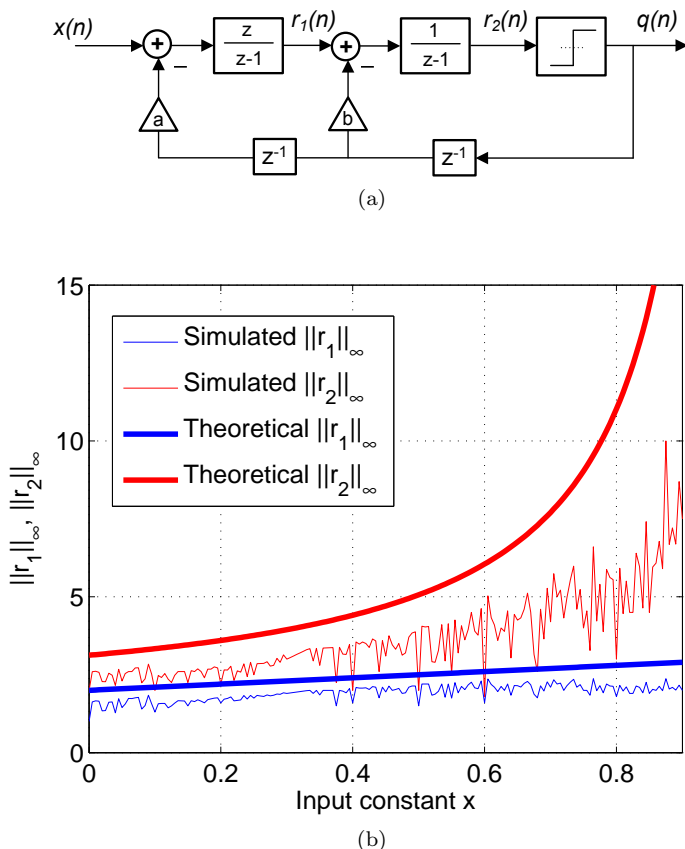


Figure 3.6: (a) A second order integrator-based low-pass $\Sigma\Delta$ -modulator with dual feedback loops. (b) Simulated $\|r_1\|_\infty$ and $\|r_2\|_\infty$ along side with theoretical state-bounds, as defined in (3.15) and (3.16).

As illustrated by simulations in Fig. 3.6b, the bounds holds for constant values of x . However, the state r_2 quickly escalates as x increases.

This approach to stability analysis has the very fundamental advantage of being exact, that is, no approximations are done at any point. However, it suffers from two major flaws. The first is that the bounds derived only are valid for a constant input, which can be sufficient for the case of high OSR in which a DC-level can be considered a good approximation of the signal. The second drawback occurs when attempting to perform the same analysis on higher order modulators. The mathematical complexity involved in analysis a higher order modulator, with non-constant input signal is highly unpractical and at times even unfeasible. Generalizations of this method have been proposed for both non-constant input and higher order modulators, [90], but it still remains that the linearized approach is often preferable even though it is approximative at best.

3.4 A Generalized Approach to $\Sigma\Delta$ -Modulator Design

Paper I presents an optimization-based method developed for selection of loop-filter coefficients in a generalized IIR-filter based $\Sigma\Delta$ -modulator structure, as illustrated in Fig. 3.7. This modulator topology is able to represent a large set of modulators, such as for example the conventional 1st and 2nd order low-pass modulators presented in the previous sections. The constant α is included in order to accommodate arbitrary input signal variance. The optimization filter $F(z)$ is chosen as to correspond to a given reconstruction filter for which we wish to minimize the post-reconstruction, residual quantization error.

The optimization algorithm uses a differentiable approximation of the quantizer in order to enable the use of gradient-based search algorithms. A damped Gauss-Newton (DGN) iteration, [91], is used to perform the search in which bandlimited Gaussian noise is used as input signal, in order to iterate toward a good set of coefficients. Finally, a Monte-Carlo based approach is used in order to overcome issues with start-value sensitivity commonly associated with the DGN for high dimensional problems.

Simulated results from one outcome of the algorithm are presented in Fig. 3.8 in terms of quantization noise PSD, in comparison with two $\Sigma\Delta$ -modulators optimized using the conventional, linearized approach. The conventional modulators are designed using the $\Sigma\Delta$ -modulator toolbox, [86], using two different stability margins - $\|\text{NTF}\|_\infty = 1.50$ for $\Sigma\Delta\#1$ and $\|\text{NTF}\|_\infty = 1.75$ for $\Sigma\Delta\#2$. The simulated reconstructed SQNR for the different modulators is plotted versus input signal variance in Fig. 3.9.

It is worth noticing that the optimized modulator shows no sign of instability during the simulations presented here, despite the fact that $\|\text{NTF}(\omega)\|_\infty \approx 2.5$, as calculated in Paper I, which clearly violates the Lee criteria. This illustrates both the inability of the Lee-criteria to accurately predict instability a priori as well as the advantage of using a non-approximative optimization algorithm, such as the one proposed in Paper I.

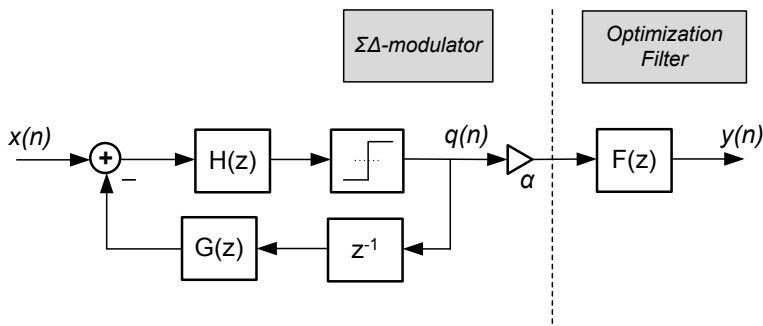


Figure 3.7: The generalized, IIR-filter based $\Sigma\Delta$ -modulator.

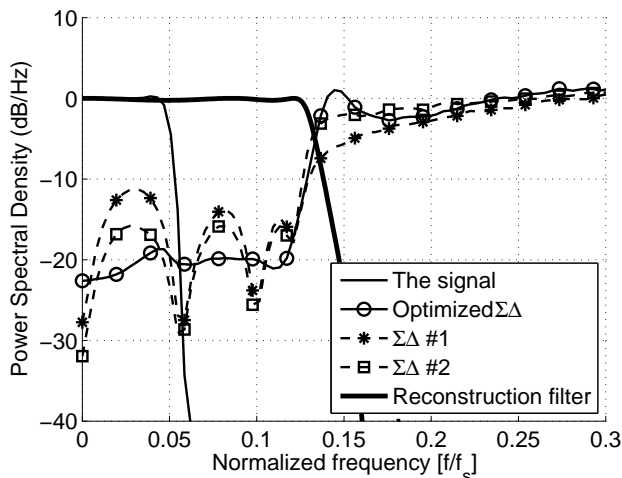


Figure 3.8: Simulations of the generalized, optimized $\Sigma\Delta$ -modulator in comparison with two modulators optimized using a conventional method with two different stability margins. The magnitude response of the optimization filter, $F(z)$, is included for comparison.

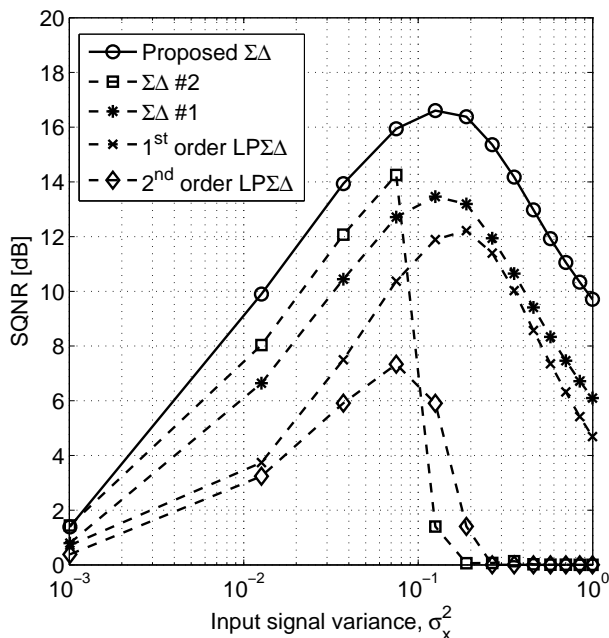


Figure 3.9: Signal to Quantization Noise Ratio (SQNR) vs input signal variance (σ_x^2) for the benchmarked $\Sigma\Delta$ implementations, here including the conventional 1st and 2nd order low-pass modulators.

3.5 Discussion

In this chapter, we have studied the concept of NSC by means of a theoretical example. Further on, the NSC scheme commonly referred to as the $\Sigma\Delta$ -modulator have been discussed and issues such as loop-filter coefficient selection and stability have been discussed. Conventional methods for design and analysis of $\Sigma\Delta$ -modulators have been reviewed. An optimization-based method for loop-filter coefficients for a generalized $\Sigma\Delta$ -modulator structure have been introduced and evaluated against the conventional methods with good results, both in terms of signal fidelity and stability.

The methods discussed in this chapter are needed in order to fully utilize the NSC features of $\Sigma\Delta$ -modulation within the context of pulsed RF transmitter architectures, which we now will move on to discuss.

Chapter 4

$\Sigma\Delta$ -Modulation for Pulsed RF Transmitters

The $\Sigma\Delta$ -modulator have found its way in to wireless communication in many different areas and aspects, both in receiver and transmitter technology, [92]. This chapter digs a little deeper into the particular use of $\Sigma\Delta$ modulation within the context of pulsed RF transmitters, as briefly introduced in Chap. 2.4. A variety of bandpass and baseband $\Sigma\Delta$ -modulation based transmitter architectures are discussed. Much of the reasoning here relies on the material presented in the previous chapter, in particular the part about STF/NTF.

First, section 4.1 covers the area of bandpass $\Sigma\Delta$ -modulation, a technology commonly suggested for direct-RF transmitters. Section 4.2 continues by surveying baseband-level RF transmitters in which $\Sigma\Delta$ -modulation is applied at baseband, before digital or analogue upconversion to RF. Finally, section 4.3 deals with three issues identified as fundamental to the use of $\Sigma\Delta$ -modulation in pulsed RF transmitters, and further introduces methods aimed to solve these issues.

4.1 RF Bandpass $\Sigma\Delta$ -Modulation

The so called bandpass $\Sigma\Delta$ -modulator can be described as a $\Sigma\Delta$ -modulator operating on a signal, whose bandpass spectrum is located around a non-zero frequency, for example - a modulated RF carrier. Thus, the poles of the modulator NTF is commonly placed around the desired frequency located at a fraction of f_s . One example of such NTF is shown in Fig. 4.1b in which the zero of the NTF is placed at $f_s/4$. These modulators directly creates a NSC encoded RF carrier which makes it quite attractive for direct-RF solutions.

However, the placement of the NTF-zero at $f_0 = f_s/N$, indicates that the modulator needs a sample-rate which is N times that of the RF carrier frequency. The need for large sample-rates are one of the weaker links in bandpass $\Sigma\Delta$ -modulation, since it results in increased power consumption of the modulator, [93]. There are however, several methods developed for finding the minimal pulse-rate needed. For example, [39] proposes a method based on a periodic signal model for selection of a sample rate which maximizes the

coding efficiency, [94], while keeping f_s at a minimum.

Despite the sample-rate requirements, research and development of bandpass $\Sigma\Delta$ -modulation based pulsed RF transmitters has been ongoing. The last few years, several examples of successful demonstrations, incorporating both analogue, [41], as well as digital modulators, [42–48], has been published.

The bandpass $\Sigma\Delta$ -modulator have further grown to be a candidate technology for frequency agile, pulsed RF transmitters, [41, 95]. These are transmitters which covers a large frequency band, non-simultaneously, which is often performed by for example re-programmable loop-filters in order to move the poles of the NTF. Concurrent multi-band transmission is however another issue, which is addressed in Chap. 4.3.3 in the context of baseband pulsed RF transmitters, a class of $\Sigma\Delta$ -modulation based transmitters we will now move on to describe.

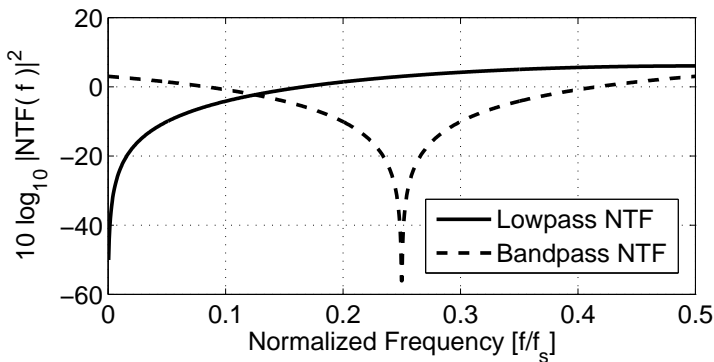
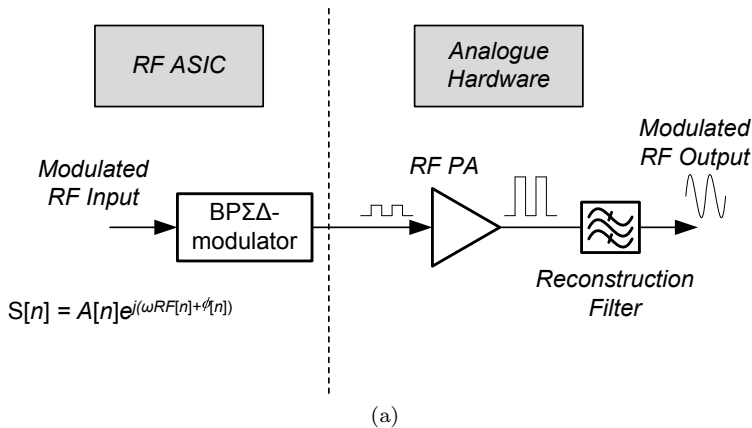


Figure 4.1: (a) A highly simplified block-schematic of a bandpass $\Sigma\Delta$ -modulator based pulsed RF transmitter. (b) NTF of both lowpass and bandpass characters with corresponding zeros at $f_0 = 0$ and $f_0 = f_s/4$.

4.2 Baseband $\Sigma\Delta$ -Modulation

This section treats RF transmitters which centers around low-pass, or base-band, $\Sigma\Delta$ -modulators, in which the zeroes of the NTF is commonly placed symmetrically around $f_s = 0$. The method in which $\Sigma\Delta$ -modulation is applied on the communication signal, is determined by the signal representation. The two common representations are based on two common coordinate systems used to describe the signals space - Quadrature and Polar,

$$S[n] = \underbrace{I[n] + iQ[n]}_{\text{Quadrature coordinates}} = \underbrace{A[n]e^{i\varphi[n]}}_{\text{Polar coordinates}} \quad (4.1)$$

The two architectures treated here will be denoted as $Q\Sigma\Delta$ and $P\Sigma\Delta$, as in Quadrature (or Cartesian in some literature) and polar. A detailed theoretical framework of general $\Sigma\Delta$ -modulation for complex-valued signals, is given in Paper II.

4.2.1 $Q\Sigma\Delta$ transmitters

The $Q\Sigma\Delta$ -transmitter is, much like the traditional quadrature transmitter, built upon applying $\Sigma\Delta$ -modulation to the real and imaginary components of the signal, before recombination, [96]. A simplified block schematic of a typical $Q\Sigma\Delta$ transmitter is shown in Fig. 4.2.

The quantizer of choice is commonly a symmetric ± 1 quantizer, which results in a constant envelope signal used to drive the RFPA with high efficiency, before the signal envelope is reconstructed by means of a linear bandpass filter.

Fig. 4.2 illustrates a $Q\Sigma\Delta$ transmitter where the upconversion of the base-band signal to RF, is performed via a mixer. However, fully digital $Q\Sigma\Delta$ implementations have been presented, for example in [97]. Here, a transmitter architecture where $\Sigma\Delta$ -modulation is applied to the real and imaginary parts at baseband before upconversion is performed using a DUC consisting of 3 MUXs, arranged as illustrated in Fig. 4.3.

However, one fundamental issue related to the $Q\Sigma\Delta$ -modulation scheme, is the poor efficiency at backed off output power operation, [56]. This is caused by

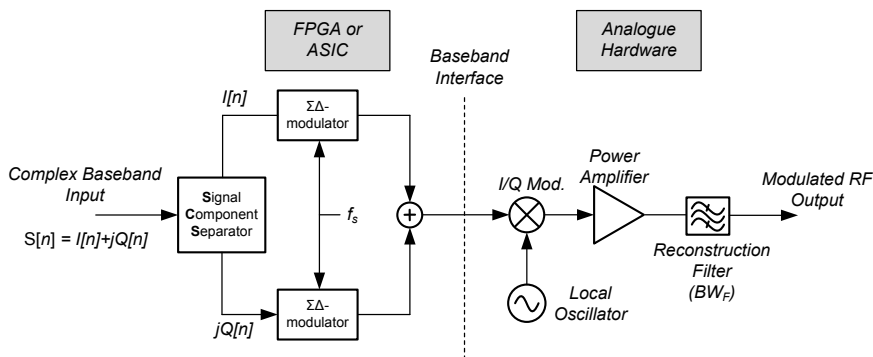


Figure 4.2: A simplified block-diagram illustrating the $Q\Sigma\Delta$ topology, which is based upon two $\Sigma\Delta$ -modulators encoding the real and imaginary parts of the signal, $S[n]$.

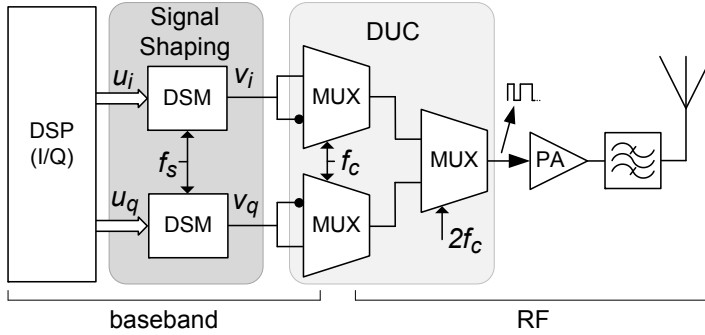


Figure 4.3: One example of a fully digital $Q\Sigma\Delta$ transmitter architecture as presented in [97]. The DUC, which consists of 3 differently clocked MUXs, provides both the combination of the quadrature components as well as the upconversion to the selected RF carrier frequency.

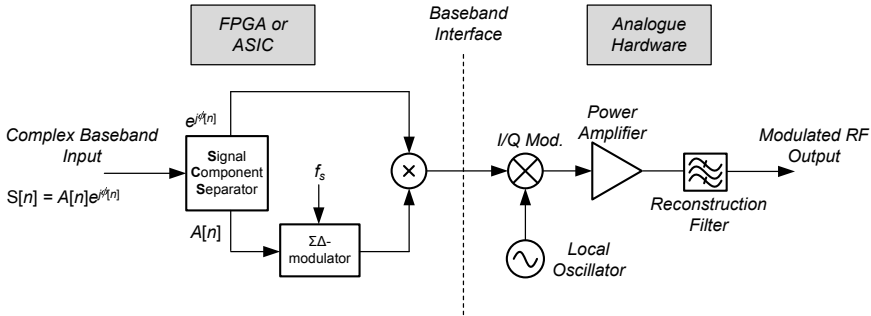


Figure 4.4: A simplified block-diagram illustrating the $P\Sigma\Delta$ topology, which is based upon one $\Sigma\Delta$ -modulator which encodes the amplitude of the signal, $S[n]$.

the lack of a zero output state which forces the modulator pair to represent any instantaneous low power signal by hopping between high power states. Thus, since most spectrally efficient communication signals are zero-mean with high PAPR, another quantization scheme might be needed, which leads us forth to the $P\Sigma\Delta$ -scheme.

4.2.2 $P\Sigma\Delta$ transmitters

The $P\Sigma\Delta$ -transmitter, as exemplified by the simple block-schematic in Fig. 4.4, utilizes a single $\Sigma\Delta$ -modulator on the amplitude component of the signal. As such, since the amplitude is strictly positive, the modulator commonly comprises a single-bit quantizer with (normalized) states $\{0, 1\}$. After recombination with the phase-component, this scheme creates what appears as bursts of phase-modulated RF carrier, which has spawned the popular name *Carrier Bursting*. Thus, contrary to the $Q\Sigma\Delta$ -scheme, the $P\Sigma\Delta$ -scheme includes a zero output state which, as shown in Paper II, greatly improves the coding efficiency.

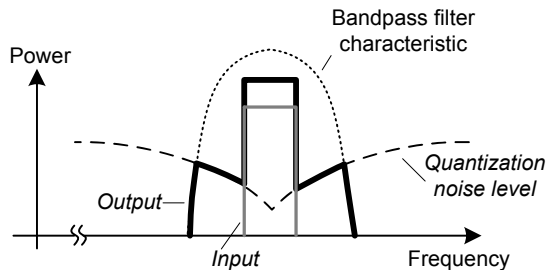


Figure 4.5: Illustration of output spectrum and reconstruction filter magnitude response.

Several successful implementations of $P\Sigma\Delta$ -modulation based RF transmitters has been demonstrated during the last decade, [9,98–101], making it a strong high efficiency RF transmitter candidate. However, there are still a few issues surrounding the $P\Sigma\Delta$ -scheme, which impedes it from being a commonly used RFPA efficiency enhancement method. The remainder of this chapter will be spent addressing a few of these issues.

4.3 Fundamental issues

In this section, three fundamental issues which hampers the performance and even the feasibility of a high performing baseband $\Sigma\Delta$ -modulation based RF transmitter is addressed. These fundamental issues relates to efficient signal reconstruction, noise-shaping properties of the polar $\Sigma\Delta$ -modulation based transmitter and concurrent multiband transmission. We will now continue to address these fundamental issues and survey methods which directly addresses them.

4.3.1 Signal Reconstruction

The largest and perhaps the most obvious issue of the pulsed RF transmitter architecture, is the inflicted need of a reconstruction filter which arises from the use of a single-bit signal representation, as illustrated in Fig. 4.5. It has been demonstrated by Wang et. al., [98], that the load impedance of the RFPA in fact changes as a function of the duty cycle, or pulse-density in the $\Sigma\Delta$ -modulation case.

Another critical issue related to the bandpass reconstruction filter, is the trade-off between filter bandwidth and pulse-rate. A larger pulse-rate will create a larger frequency range in which the SQNR is high and thus, a more wideband reconstruction filter with less insertion loss can be used. But due to the fact that no RF power transistor is an ideal switch, power losses will occur due to parasitic elements present in the non-ideal device.

In order to exemplify, we can simply study the theoretical SQNR of a first order low-pass modulator which, as stated in Paper II, can be estimated using

the modulator NTF as

$$\text{SQNR} = 10 \log_{10} \frac{\sigma^2}{\sigma_q^2 \int_0^{\frac{\omega_0}{\omega_s}} |\text{NTF}(\omega)|^2 d\omega} = 10 \log_{10} \frac{\sigma^2}{\sigma_q^2 \left(\frac{\omega_0}{\omega_s} - \sin \frac{\omega_0}{\omega_s} \right)} \quad (4.2)$$

where σ^2 is the input signal variance, σ_q^2 is the quantization noise power, $\omega_0 = 2\pi f_0$ is the cutoff frequency of the reconstruction filter and $\omega_s = 2\pi f_s$ is the sample-rate. It is clear that the SNR can be improved by increasing the sample-rate of the modulator. However, high pulse-rates increases the switch-loss, which according to a simple switch-model, can be described by

$$P_{\text{diss}}(f) = f_s C_s V_{DD}^2 \quad (4.3)$$

where $f_s \gg f_0$ is the pulse-rate, C_s is the parasitic switch capacitance and V_{DD} is the supply voltage. In RFPA terms, C_s can be considered equivalent to that of the output capacitance of the transistor and V_{DD} the drain-voltage. These two simple equations illustrates the need of keeping the pulse-rates to a minimum. Further, it illustrates the difficulty of scaling in terms of power, since either C_s or V_{DD} will increase as the maximum power increases.

The requirements on the reconstruction filter bandwidth can however be relaxed using the system shown in Fig. 4.6. Here, the resulting quantization noise from the $\Sigma\Delta$ -modulation based carrier bursting part, as indicated in the system diagram, is filtered by the low-pass filter $F(z)$ and superimposed back on to the signal. This will effectively cancel out the quantization noise located around the modulated RF carrier, at a bandwidth determined by $F(z)$, as sketched in Fig. 4.7 where the cancellation bandwidth is denoted BW_c .

The resulting signal will, due to the single-bit modulation of the envelope, have a bi-modal mixture PDF as illustrated in Fig. 4.8. The components of the mixture will be Rice-distributed, provided that the filtered quantization noise used for suppression, is Gaussian. As a result, the RFPA is only operated over regions in which the power efficiency is fairly high. In order to further improve the efficiency, an amplitude limitation and normalization stage is added, as

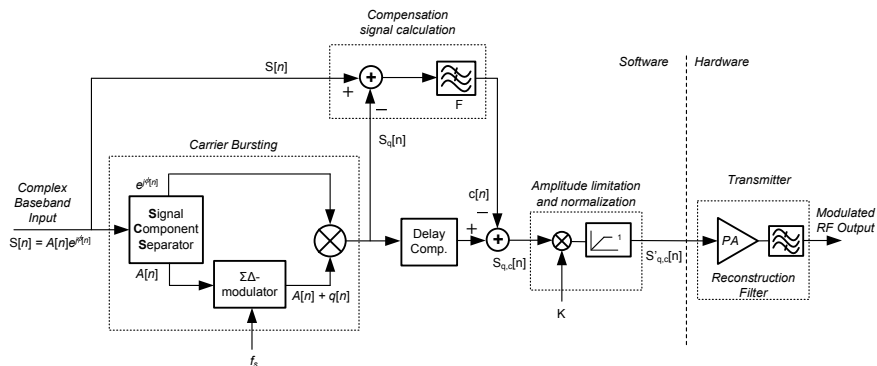


Figure 4.6: The pre-compensation based quantization noise cancellation system as proposed in Paper II, here for a Carrier bursting system.

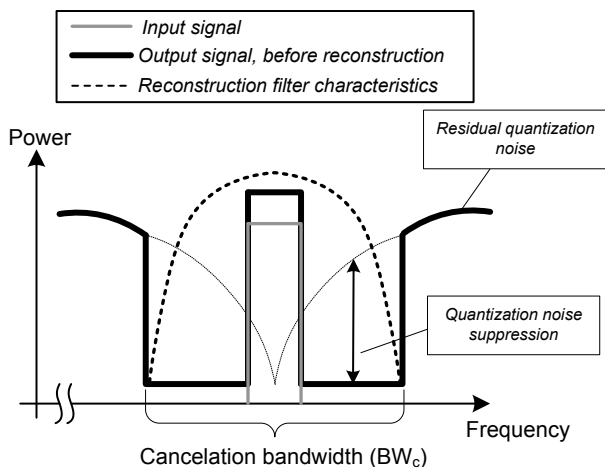


Figure 4.7: A principal sketch of the resulting PSD of the $\Sigma\Delta$ -modulated signal, before and after application of the suppression component which clears the frequency span, BW_c , from quantization noise.

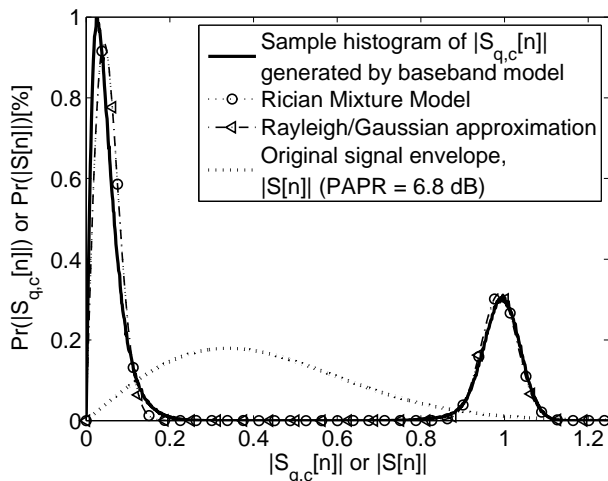


Figure 4.8: The resulting Rician envelope distributions after applied $\Sigma\Delta$ -modulation and partial quantization noise cancellation. Here shown along side with the Rayleigh/Gaussian approximation used for the analytical model in Paper II, and the PDF of the original envelope.

shown in Fig. 4.6. An additive white Gaussian noise (AWGN) model of the clipping noise, is derived in order to predict the spectral regrowth caused by the clipping process.

Further on, as a part of the theoretical framework presented in Paper II, the variance of the Rician mixture components is shown to be dependent on the compensation signal bandwidth, as well as the noise-shape of the $\Sigma\Delta$ -modulator. It is shown in great detail, both theoretically and experimentally,

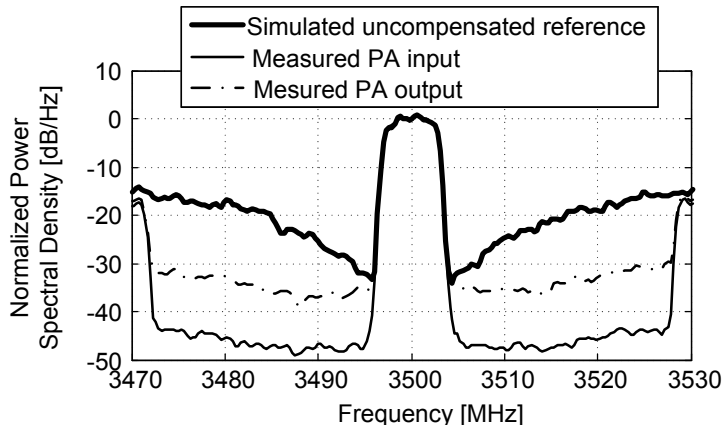


Figure 4.9: One example of measured PSD of the RFPA input and output signal. Here, the pulse-rate is set to 100 MHz, using a compensation bandwidth of 40 MHz.

how the optimization algorithm presented in Paper I allows for efficiency optimization of the proposed system. The method has been experimentally evaluated using two different RFPA, operating at two different center frequencies, as presented in [a] and Paper II. Fig. 4.9 shows one example of how the quantization noise is suppressed from the frequency band surrounding the RF carrier. The introduced amplitude variations causes spectral regrowth due to the nonlinear RFPA, which needs to be handled. Measurements taken in [a] shows the possibility of deploying a digital pre-distorter (DPD) in order to recover the desired spectrum.

4.3.2 Noise-Shaping Properties in Polar Transmitters

One fundamental issue of the $P\Sigma\Delta$, is the corruption of the desired quantization noise spectra caused by the recombination of the $\Sigma\Delta$ -modulated amplitude with the phase-component. The convolution of the two frequency spectrum's reduces the impact of the NTF zeros on the final SQNR. This effect is exemplified in Fig. 4.10, and is usually only visible when plotting the spectrum of the quantization noise separately. This issue is unique to the $P\Sigma\Delta$ -scheme since, for the $Q\Sigma\Delta$, orthogonality of the two components eases dividing and recombining the signal due to the lack of nonlinear operations.

As shown in Paper III, the output spectrum of the $P\Sigma\Delta$ -modulation scheme can be written as

$$\Phi_{\hat{S}}(\omega) = \Phi_S(\omega) + \sigma_e^2 |\Phi_\varphi(\omega) \otimes \text{NTF}(\omega)|^2 \quad (4.4)$$

where $\Phi_\varphi(\omega)$ is the PSD of the phase-component and \otimes is the convolution operator. And, since $\Phi_\varphi(\omega)$ can safely be assumed to have a non-flat spectrum, the resulting shape of the quantization noise will suffer, as shown in Fig. 4.10.

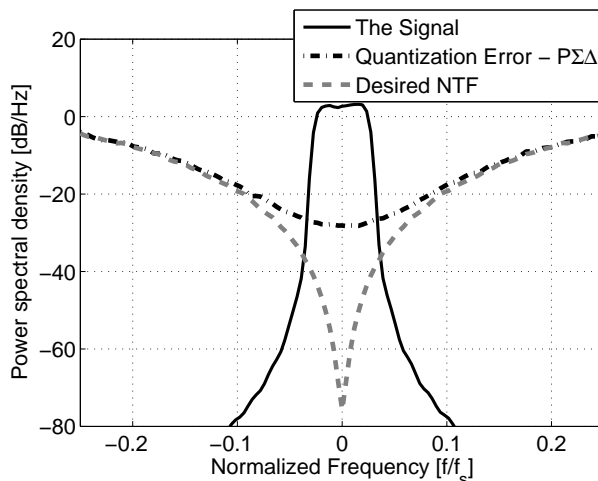


Figure 4.10: A simulated example of the quantization noise shape corruption taking place in the conventional $P\Sigma\Delta$ transmitter, in comparison with the desired NTF.

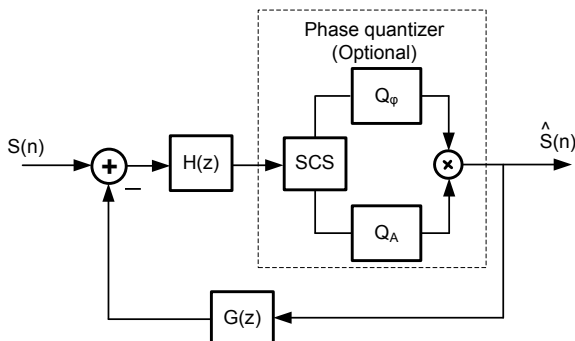


Figure 4.11: A generalized version of the $\mathbb{C}\Sigma\Delta$ -modulator, as presented in Paper II.

One remedy to the issue of corrupted NSC properties comes in the form of a complex $\Sigma\Delta$ -modulator, $\mathbb{C}\Sigma\Delta$, which is presented and analyzed in detail in Paper III. The developed modulator concept incorporates the whole complex signal, including the phase-component, into the feedback loop which in turns leads to preserved NSC properties of the resulting signal representation. This particular issue has been briefly addressed in [102], but with little substantial analysis of either the root cause or the solution. Paper III further provides a theoretical framework for $\Sigma\Delta$ -modulation of complex-valued signals in general.

In addition to the improved noise-shaping properties of the $\mathbb{C}\Sigma\Delta$ -modulator, there follows a possibility to introduce a coarse quantization of the phase-component. The effects of the coarsely quantized phase-component is partially mitigated by the noise-shaping mechanism, in the same manner as the amplitude quantization error. Thus, the $\mathbb{C}\Sigma\Delta$ -modulator enables a low resolution quantization of the complex signal with good SQNR.

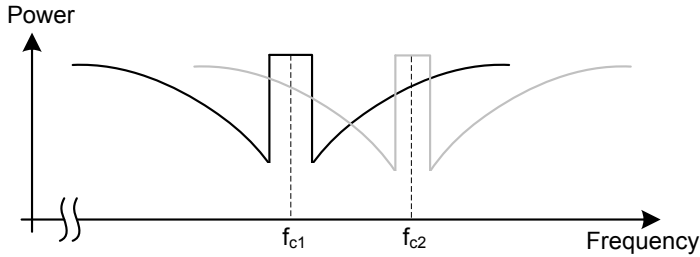


Figure 4.12: Overlapping spectrum of two $\Sigma\Delta$ -modulator encoded RF carriers.

The modulator described in Paper III can be generalized in the same manner as the real-valued modulator in Paper I. Such a modulator is shown in Fig. 4.11, where $H(z)$ and $G(z)$ are IIR-filters with real-valued coefficients. Paper II further illustrates how the algorithm presented in Paper I can be modified in order to optimize the IIR loop filter coefficients of the generalized $\mathbb{C}\Sigma\Delta$ -modulator. The modification mainly consists of adapting the differentiable quantizer approximation, which is needed to perform the damped Gauss-Newton search. As shown in Paper III, the optimized $\mathbb{C}\Sigma\Delta$ -modulator shows not only excellent performance in terms of SQNR, in comparison with the other simulated modulators, but also good stability performance.

4.3.3 Concurrent Multiband Transmission

Historically, the $\Sigma\Delta$ -modulation based transmitters have not been considered very strong candidates when it comes to concurrent multi-band transmission, much due to the extreme wideband nature of the single-bit quantized signal. As illustrated in Fig. 4.12, the quantization noise from one carrier might overlap with the desired signal from the other carrier, if special care of the quantization noise shapes is not taken while designing the system.

It is possible to design so called multi-band $\Sigma\Delta$ -modulators, [103], which as the name suggests are modulators whose NTF contains more than one stop-band. This method does however suffer from several drawbacks. First, the sample-rate in which the modulator operates needs to be very large in order to accommodate the wide frequency range of operation. Secondly, the number of poles needed in the modulator design multiplies with the number of stop-band of the NTF, which increases the difficulty in stabilizing the modulator. Architectures which uses these types of modulators have been proposed in the past, [104, 105], but more recent results are lacking.

Examples of how a highly reconfigurable, multi-band transmitter can be achieved by means of low-pass $\Sigma\Delta$ -modulation is provided in Paper IV. Here, second order low-pass modulators of Cascade-of-Resonators with distributed Feed-Forward (CRFF) type with an OSR of 12.5 were optimized using the MATLAB $\Sigma\Delta$ -modulator toolbox, [86].

Each carrier is produced by first encoding the baseband signals using individual pairs of $\Sigma\Delta$ -modulators, before combining them using the interconnection network, as illustrated in Fig. 4.13a. This network is configured to generate a N -bit word which consists of interleaved output values from the

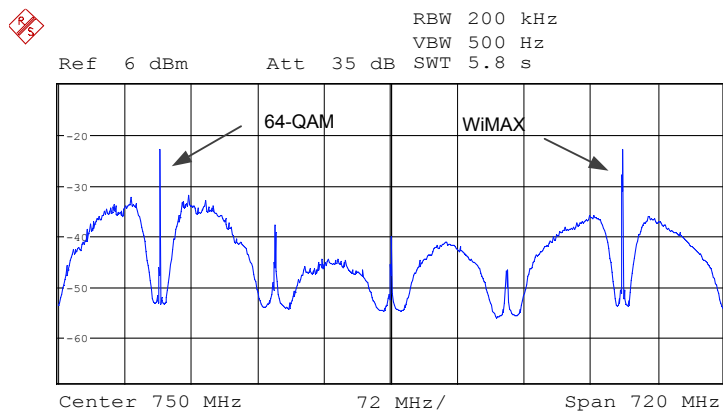
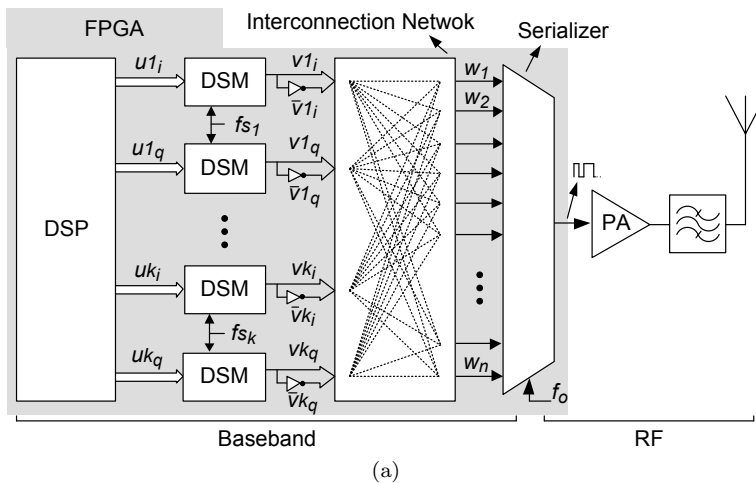


Figure 4.13: (a) A concurrent multi-band $\Sigma\Delta$ -modulator based RF transmitter as presented in Paper IV. (b) Measurement of a dual-carrier (64 QAM at 500 MHz, WiMAX at 1 GHz).

different $\Sigma\Delta$ -modulators, as illustrated in Fig. 4.13a. This is then serialized creating a high-speed, single-bit data-stream. Paper IV illustrates how the N -bit word can be configured in order to select the carrier frequencies for each carrier.

The system were experimentally evaluated on a Virtex6 VLX240T Field Programmable Gate-Array (FPGA) evaluation board. Measurements were made using a dual-carrier signal which contained two carriers - a 64-QAM signal centered at 1 GHz and a 1.25 MHz wide WiMAX signal centered at 500 MHz, as exemplified in Fig. 4.13b.

4.4 Discussion

This chapter discussed the use of $\Sigma\Delta$ -modulation in the context of pulsed RF transmitters, both at RF- and baseband-level. Three fundamental issues have been identified and methods aimed toward solving them has been discussed. A pre-compensation based method enabling the use of wideband reconstruction filters has been studied, both theoretically and experimentally. A theoretical framework of the proposed architecture is presented, providing tools for efficiency optimization.

Further on, an issue of noise-shape corruption have been identified in the context of polar $\Sigma\Delta$ -modulation based transmitters. A complex $\Sigma\Delta$ -modulator is shown to remedy this issue by incorporating the complex signal in its entirety in the noise-shaping feedback loop. As a result, it is possible to introduce a low-resolution phase-quantization scheme, reducing the total number of bits required to accurately represent the signal after reconstruction.

Finally, a transmitter architecture enabling multi-carrier transmission were discussed. The architecture is based upon a set of quadrature $\Sigma\Delta$ -modulation pairs and a interconnection network, which forms an N -bit word containing interleaved values from each $\Sigma\Delta$ -modulator, from which the multi-carrier signal is formed using a serializer.

Chapter 5

Conclusions and Future Work

5.1 Conclusions

This thesis treats the use of Noise-Shaped Coding by means of $\Sigma\Delta$ -modulation as an efficiency enhancement technique in conjunction with pulsed RF transmitter architectures.

Important efficiency metrics and common efficiency enhancement techniques such as dynamic load and supply modulation have been reviewed. The pulsed RF transmitter architecture has been introduced in its two most common forms.

Noise-Shaped Coding has been introduced, with focus on the $\Sigma\Delta$ -modulator as the most common method of implementation. Conventional methods for a priori predicting performance and stability in $\Sigma\Delta$ -modulators have been reviewed. An optimization based approach to $\Sigma\Delta$ -modulator design has been proposed. The method is built around a generalized IIR-filter based $\Sigma\Delta$ -modulator and a differentiable quantizer approximation, which in turn enables the use of a damped Gauss-Newton search. The optimized modulator was benchmarked against modulators designed using conventional tools, showing improvements both in terms of post-reconstruction signal purity as well as stable input signal range.

A fundamental issue regarding the noise-shaping properties in polar $\Sigma\Delta$ -modulator based pulsed RF transmitters is identified. A remedy is proposed in terms of a complex $\Sigma\Delta$ -modulator, which operates directly on the complex signal, without any extrinsic signal separation process. This provides a better a priori control of the quantization noise shape as well as improved signal fidelity.

Following the discussion on Noise-Shaped Coding, the thesis continues by introducing the different approaches of applying single-bit $\Sigma\Delta$ -modulation in the context of pulsed transmitter architectures. Both RF and baseband methods are discussed and important issues related to their implementation are identified. A method designed to suppress parts of the quantization noise around the modulated RF carrier by means of a variance-limited amplitude

component, enabling the use of a more wideband reconstruction filter, is proposed. The method is analyzed mathematically in terms of an ideal class B based efficiency model and evaluated experimentally on two different high efficiency RFPAs. It is further shown how the previously proposed optimization-based $\Sigma\Delta$ -modulator design approach can be used in order to optimize the performance of the proposed suppression method. This is done by minimizing the in-band quantization noise which, in turn, reduces the superimposed amplitude variations, increasing the RFPA power efficiency.

The work presented in this thesis contributes to the advancement in development of $\Sigma\Delta$ -modulation based pulsed RF transmitters by addressing some of their fundamental limitations.

5.2 Future work

The work presented in this thesis can be extended in any of the following ways.

First, the single most important issue still posing a potential threat to a successful implementation of a $\Sigma\Delta$ -modulator based pulsed RF transmitter, is the process of reconstructing the signal in an efficient manner. This thesis has been focused on investigating methods in the area of $\Sigma\Delta$ -modulation and signal processing aimed at relieving the filtering issue in terms of reduced insertion loss. For an efficient signal reconstruction however, the undesired load-modulation effect taking place, needs to be addressed further by means of a co-designed RFPA/filter solution. The Doherty-based solution posed by Wang et. al., [98], is of interest, but as discussed in Chap. 2, the Doherty suffers from bandwidth limitations due to the $\lambda/4$ -transmission line. The Doherty amplifier do however open up for a 3-level carrier bursting scheme, which would reduce the total amount of quantization noise produced.

Further on, a theoretical issue which needs to be addressed, is a lower bound for the post-reconstruction SQNR for the oversampled, single-bit quantization problem. This would provide some insight in exactly how well the $\Sigma\Delta$ -modulator performs and, ultimately, if further research on the area of single-bit noise-shaped coding schemes is needed or if the $\Sigma\Delta$ -modulator is "good enough".

Chapter 6

Summary of Appended Papers

Paper I

Quantization Noise Minimization in $\Sigma\Delta$ -modulation based RF Transmitter Architectures

This paper presents a novel approach to loop-filter coefficient selection in $\Sigma\Delta$ -modulator design. The algorithm is developed around a generalized IIR-filter based modulator structure, a differentiable quantizer approximation and the damped Gauss-Newton iteration.

My contributions are: Design, analysis, implementation and evaluation of the optimization algorithm. Authoring the paper.

Paper II

An RF Carrier Bursting System using Partial Quantization Noise Cancellation

This paper presents a pre-compensation based method aimed to increase the passband of the reconstruction filter, in order to reduce its insertion loss and thus, increase the power efficiency. The method is analyzed by means of the statistical signal properties, in conjunction with an ideal class-B amplifier model. The theoretical model is used in order to identify and illustrate efficiency trends as a function of system design parameters such as compensation signal bandwidth and clipping probability. Finally, the concept is experimentally validated using a high efficiency inverse class F RF power amplifier.

My contributions are: Design, mathematical analysis and experimental evaluation of the proposed system. Authoring the paper.

Paper III

On $\Sigma\Delta$ -Modulation of Quadrature Signals

This paper presents a detailed treatment of different baseband $\Sigma\Delta$ -modulation schemes, as applied to quadrature communication signals, using both in a Cartesian and polar signal representation. For the polar case, it is shown that the noise-shaping properties of the $\Sigma\Delta$ -modulator are corrupted by the recombination of the amplitude- and the phase-components. For this reason, a new modulator structure is presented, which preserves the noise-shaping properties and thus, improves the signal-to-noise ratio

My contributions are: Mathematical analysis and simulation-based evaluation of the different modulator concepts. Authoring the paper.

Paper IV

A Novel All-Digital Multichannel Multimode RF Transmitter Using $\Sigma\Delta$ -modulation

This paper presents a dual-band $\Sigma\Delta$ -modulator based RF transmitter, implemented on an Xilinx Virtex6 VLX240T FPGA.

My contributions are: Selection of a suitable $\Sigma\Delta$ -modulator topology and loop-filter coefficient optimization for implementation on the FPGA platform.

Acknowledgment

Working toward a Ph.D degree seemed at times as a lonesome task. However, without the support of some remarkable people, I would not have made it this far.

I would like to thank my examiner and head of Microwave Electronics Lab., Prof. Herbert Zirath, for taking me in as a Ph.D student and providing a rich, academic environment within which I was able to grow toward an independent researcher.

To my supervisor, Prof. Thomas Eriksson, and my co-supervisor, Dr. Christian Fager, I owe a great deal of gratitude for their day to day support which amongst many things has included countless discussions, not always ending in agreement. Thank you for your patience!

To all my friends, colleagues, managers, mentors and sponsors at Ericsson AB, Stockholm - in particular to Dr Peter Olanders, Bo G. Berglund, Hannes Medelius, Johan Thorebäck, Thomas Lejon, Nedzad Lekic, Torbjörn Thunell and Pär Schöldström, for all their wisdom and support during these years.

Thanks to Prof. Jan Grahn for providing the stimulating research environment which is the GigaHertz Centre.

To my gracious hosts at the University of Aveiro, Portugal, for taking good care of me during my research visit. Most of all, I am very grateful for the time I got to spend with Prof. José-Carlos Pedro, who is simply an inexhaustible source of great ideas. Also, big thanks to Telmo Cunha, Pedro Cabral, Pedro Lavrador, Nelson Silva and Nuno Borghes Carvalho.

Thanks to all my Ph.D student colleagues at the Microwave Electronics Lab and the Communication Systems group.

Thanks to my neighbor, Adj. Prof. Rik Jos of NXP, Nijmegen, for all the discussions on topics such as conformal mappings and glögg.

Thanks to my parents, Jörgen and Christina, and to Felix and Maria for all their love and support.

Finally, to my Linnéa - for always putting a smile on my face and for making me feel loved. I love you and I would be lost without you!

This research was carried out at the GigaHertz Centre in joint projects supported by the Swedish Governmental Agency for Innovation Systems (VINNOVA), Chalmers University of Technology, ComHeat Microwave AB, Ericsson AB, Infineon Technologies Austria AG, Mitsubishi Electric Corporation, NXP Semiconductors BV, Saab AB, and the SP Technical Research Institute of Sweden.

Bibliography

- [1] B. Leiner, V. Cerf, D. Clark, R. Kahn, L. Kleinrock, D. Lynch, J. Postel, L. Roberts, and S. Wolff, "A brief history of the internet." [Online]. Available: <http://www.isoc.org/internet/history/brief.shtml>
- [2] "More than 50 billion connected devices - Taking connected devices to mass market and profitability," White paper, Ericsson AB, 2011.
- [3] "Cisco visual networking index: Global mobile data traffic forecast update, 2010-20115," White paper, Cisco, 2011.
- [4] E. Dahlman, S. Parkwall, J. Sköld, and P. Beming, "*3G Evolution HSPA and LTE for Mobile Broadband*". Academic Press, ISBN 978-0-12-374538-5, 2008.
- [5] "Energy Logic for Telecommunications," White paper, Emerson Network Power, Sept. 2008.
- [6] P. Lavrador, T. Cunha, P. Cabral, and J. Pedro, "The linearity-efficiency compromise," *Microwave Magazine, IEEE*, vol. 11, no. 5, pp. 44–58, Aug. 2010.
- [7] E. Buracchini, "The software radio concept," *Communications Magazine, IEEE*, vol. 38, no. 9, pp. 138–143, Sep 2000.
- [8] F. Ghannouchi, "Power amplifier and transmitter architectures for software defined radio systems," *Circuits and Systems Magazine, IEEE*, vol. 10, no. 4, pp. 56 –63, fourthquarter 2010.
- [9] F. H. Raab, P. Asbeck, S. Cripps, P. B. Kenington, Z. B. Popovic, N. Potheary, J. F. Sevic, and N. O. Sokal, "RF and microwave power amplifier and transmitter technologies - part 5," *High Frequency Electronics*, vol. 3, no. 1, pp. 46 – 54, Jan. 2004.
- [10] L. Kahn, "Single-sideband transmission by envelope elimination and restoration," *Proceedings of the IRE*, vol. 40, no. 7, pp. 803–806, July 1952.
- [11] F. Raab, "Split-band modulator for kahn-technique transmitters," vol. 2, June 2004, pp. 887–890 Vol.2.

- [12] H. M. Nemati, C. Fager, M. Thorsell, and H. Zirath, "Characterization of switched mode LDMOS and GaN power amplifiers for optimal use in polar transmitter architectures," *Microwave Symposium Digest, 2008 IEEE MTT-S International*, 2008.
- [13] J. Jeong, D. Kimball, M. Kwak, C. Hsia, P. Draxler, and P. Asbeck, "Modeling and design of RF amplifiers for envelope tracking wcdma base-station applications," *IEEE Trans. Microw. Theory Tech.*, vol. 57, no. 9, pp. 2148–2159, sept. 2009.
- [14] J. Pedro, J. Garcia, and P. Cabral, "Nonlinear distortion analysis of polar transmitters," *IEEE Trans. Microw. Theory Tech.*, vol. 55, no. 12, pp. 2757–2765, dec. 2007.
- [15] W. Doherty, "A new high efficiency power amplifier for modulated waves," *Proceedings of the IRE*, vol. 24, no. 9, pp. 1163–1182, Sept. 1936.
- [16] M. Pelk, W. Neo, J. Gajadharsing, R. Pengelly, and L. de Vreede, "A high-efficiency 100-w gan three-way doherty amplifier for base-station applications," *IEEE Trans. Microw. Theory Tech.*, vol. 56, no. 7, pp. 1582–1591, July 2008.
- [17] A. Grebennikov, "*RF and Microwave Power Amplifier Design*", 1st ed. McGraw-Hill, 2005.
- [18] P. Kenington, "*High-Linearity RF Amplifier Design*". Boston: Artech House Publishers, 2000.
- [19] W. Chen, S. Bassam, X. Li, Y. Liu, K. Rawat, M. Helaloui, F. Ghannouchi, and Z. Feng, "Design and linearization of concurrent dual-band doherty power amplifier with frequency-dependent power ranges," *IEEE Trans. Microw. Theory Tech.*, vol. 59, no. 10, pp. 2537–2546, Oct. 2011.
- [20] M. Nick and A. Mortazawi, "Adaptive input-power distribution in Doherty power amplifiers for linearity and efficiency enhancement," *IEEE Trans. Microw. Theory Tech.*, vol. 58, no. 11, pp. 2764–2771, Nov. 2010.
- [21] R. Darraji and F. M. Ghannouchi, "Digital doherty amplifier with enhanced efficiency and extended range," *IEEE Trans. Microw. Theory Tech.*, vol. PP, no. 99, p. 1, 2011.
- [22] H. Chireix, "High power outphasing modulation," *Proceedings of the IRE*, vol. 23, no. 11, pp. 1370–1392, Nov. 1935.
- [23] D. Perreault, "A new power combining and outphasing modulation system for high-efficiency power amplification," *IEEE Trans. Circuits Syst. I*, vol. 8, no. 8, pp. 1713–1726, Aug. 2011.
- [24] D. Cox, "Linear amplification with nonlinear components," *IEEE Trans. Commun.*, vol. 22, no. 12, pp. 1942–1945, dec 1974.
- [25] X. Zhang, L. Larson, and P. Asbeck, "*Design of Linear RF Outphasing Power Amplifiers*", 1st ed. Artech House, 2003.

- [26] M. Helaoui, S. Boumaiza, F. Ghannouchi, A. Kouki, and A. Ghazel, "A new mode-multiplexing linc architecture to boost the efficiency of wimax up-link transmitters," *IEEE Trans. Microw. Theory Tech.*, vol. 55, no. 2, pp. 248 – 253, Feb. 2007.
- [27] F. Raab, "High-efficiency linear amplification by dynamic load modulation," vol. 3, June 2003, pp. 1717–1720 vol.3.
- [28] H. M. Nemati, "High-efficiency power amplification techniques for wireless transmitters," Ph.D. dissertation, Chalmers University of Technology, 2010.
- [29] H. T. Jeong, H. S. Lee, I. S. Chang, and C. D. Kim, "Efficiency enhancement method for high-power amplifiers using a dynamic load adaptation technique," in *Microwave Symposium Digest, 2005 IEEE MTT-S International*, june 2005, p. 4 pp.
- [30] J. Jeong and P. Asbeck, "Efficiency ehancement of w-cdma base-station envelope tracking power amplifiers via load modulation," *Microwave and Optical Technology Letters*, vol. 49, no. 8, pp. 1954–1957, 2007. [Online]. Available: <http://dx.doi.org/10.1002/mop.22566>
- [31] A. Tehrani, H. Nemati, H. Cao, T. Eriksson, and C. Fager, "Dynamic load modulation of high power amplifiers with varactor-based matching networks," in *Microwave Symposium Digest, 2009. MTT '09. IEEE MTT-S International*, june 2009, pp. 1537 –1540.
- [32] K. Buisman, L. de Vreede, L. Larson, M. Spirito, A. Akhnoukh, Y. Lin, X. Liu, and L. Nanver, "Low-distortion, low-loss varactor-based adaptive matching networks, implemented in a silicon-on-glass technology," in *Radio Frequency integrated Circuits (RFIC) Symposium, 2005. Digest of Papers. 2005 IEEE*, june 2005, pp. 389 – 392.
- [33] H. Cao, H. Nemati, A. Tehrani, T. Eriksson, J. Grahn, and C. Fager, "Linearization of efficiency-optimized dynamic load modulation transmitter architectures," *IEEE Trans. Microw. Theory Tech.*, vol. 58, no. 4, pp. 873 –881, april 2010.
- [34] H. Cao, C. Fager, T. Khan, A. Tehrani, and T. Eriksson, "Comparison of bandwidth reduction schemes in dynamic load modulation power amplifier architectures," in *Integrated Nonlinear Microwave and Millimetre-Wave Circuits (INMMIC), 2011 Workshop on*, april 2011, pp. 1 –4.
- [35] H. Cao, A. Tehrani, H. Nemati, C. Fager, T. Eriksson, and H. Zirath, "Time alignment in a dynamic load modulation transmitter architecture," in *Microwave Conference, 2009. EuMC 2009. European*, 29 2009-oct. 1 2009, pp. 1211 –1214.
- [36] M. Levy, "Pulse modulation and demodulation theory," *Radio Engineers, Journal of the British Institution of*, vol. 7, no. 2, pp. 64 –83, march-april 1947.

- [37] D. Schdnung and H. Stemmler, "Geregelter drehstrom-umkehrantrieb mit gesteuertem umrichter nach dem unterschwingungsverfahren," *Brown Boveri Mitt.*, vol. 51, pp. 555–577, 1964.
- [38] J. Gregory, "Power amplifier employing pulse duration modulation," US Patent 3.260.912, 1966.
- [39] T. Johnson and S. Stapleton, "Comparison of bandpass $\Sigma\Delta$ modulator coding efficiency with a periodic signal model," *IEEE Trans. Circuits Syst. II*, vol. 55, no. 11, pp. 3763–3775, Dec. 2008.
- [40] T. Johnson and S. P. Stapleton, "RF class-D amplification with band-pass $\Sigma\Delta$ -modulator drive signals," *IEEE Trans. Circuits Syst. I*, vol. 53, no. 12, pp. 2507–2520, dec. 2006.
- [41] M. Schmidt, M. Grozing, S. Heck, I. Dettmann, M. Berroth, D. Wiegner, W. Templ, and A. Pascht, "A 1.55 ghz to 2.45 ghz center frequency continuous-time bandpass delta-sigma modulator for frequency agile transmitters," in *Radio Frequency Integrated Circuits Symposium, 2009. RFIC 2009. IEEE*, Jun. 2009.
- [42] J. Keyzer, J. Hinrichs, A. Metzger, M. Iwamoto, I. Galton, and P. Asbeck, "Digital generation of rf signals for wireless communications with band-pass delta-sigma modulation," in *Microwave Symposium Digest, 2001 IEEE MTT-S International*, vol. 3, June 2001, pp. 2127 – 2130.
- [43] A. Frappe, A. Flament, B. Stefanelli, A. Kaiser, and A. Cathelin, "An all-digital RF signal generator using high-speed $\Delta\Sigma$ -modulators," *IEEE J. Solid-State Circuits*, vol. 44, no. 10, pp. 2722–2732, oct. 2009.
- [44] A. Frappe, A. Flament, B. Stefanelli, A. Cathelin, and A. Kaiser, "All-digital RF signal generation for software defined radio," in *Circuits and Systems for Communications, 2008. ECCSC 2008. 4th European Conference on*, july 2008, pp. 236 –239.
- [45] A. Frappe, A. Flament, A. Kaiser, B. Stefanelli, and A. Cathelin, "Design techniques for very high speed digital delta-sigma modulators aimed at all-digital rf transmitters," in *Electronics, Circuits and Systems, 2006. ICECS '06. 13th IEEE International Conference on*, dec. 2006, pp. 1113 –1116.
- [46] A. Frappe, B. Stefanelli, A. Flament, A. Kaiser, and A. Cathelin, "A digital $\Delta\Sigma$ RF signal generator for mobile communication transmitters in 90nm CMOS," 17 2008-April 17 2008, pp. 13–16.
- [47] J. Ketola, J. Sommarek, J. Vankka, and K. Halonen, "Transmitter utilising bandpass delta-sigma modulator and switching mode power amplifier," in *Circuits and Systems, 2004. ISCAS '04. Proceedings of the 2004 International Symposium on*, 2004.
- [48] J. Sommarek, J. Vankka, J. Ketola, J. Lindeberg, and K. Halonen, "Digital modulator with bandpass delta-sigma modulator," *Analog Integrated*

- Circuits and Signal Processing*, vol. 43, pp. 81–86, 2005, 10.1007/s10470-005-6573-z. [Online]. Available: <http://dx.doi.org/10.1007/s10470-005-6573-z>
- [49] F. Raab, “Radio frequency pulsewidth modulation,” *IEEE Trans. Commun.*, vol. 21, no. 8, pp. 958–966, Aug. 1973.
- [50] M. Ozen, R. Jos, C. M. Andersson, M. Acar, and C. Fager, “High-efficiency RF pulsewidth modulation of class-e power amplifiers,” *IEEE Trans. Microw. Theory Tech.*, vol. PP, no. 99, p. 1, 2011.
- [51] M. Ozen, C. Andersson, M. Thorsell, K. Andersson, N. Rorsman, C. Fager, M. Acar, M. van der Heijden, and R. Jos, “High efficiency RF pulse width modulation with tunable load network class-e pa,” in *Wireless and Microwave Technology Conference (WAMICON), 2011 IEEE 12th Annual*, april 2011, pp. 1–6.
- [52] M. Nielsen and T. Larsen, “An RF pulse width modulator for switch-mode power amplification of varying envelope signals,” *SiRF*, 2007.
- [53] B. Hart, “*Introduction to analogue electronics*”. Butterworth-Heinemann Ltd., 1996.
- [54] C. Schubert, P. Singerl, M. Gadringer, H. Arthaber, A. Wiesbauer, and G. Magerl, “Highly efficient switched-mode transmitter using a current mode class-D RF amplifier,” *International Journal of RF and Microwave Computer-Aided Engineering*, vol. 20, no. 4, pp. 446–457, May 2010.
- [55] C. Berland, I. Hibon, J. Bercher, M. Villegas, D. Belot, D. Pache, and V. Le Goasoz, “A transmitter architecture for nonconstant envelope modulation,” *IEEE Trans. Circuits Syst. II*, vol. 53, no. 1, pp. 13–17, Jan. 2006.
- [56] F. Ghannouchi, S. Hatami, P. Aflaki, M. Helaoui, and R. Negra, “Accurate power efficiency estimation of GHz wireless $\Delta\Sigma$ transmitters for different classes of switching mode power amplifiers,” *IEEE Trans. Microw. Theory Tech.*, vol. 58, no. 11, pp. 2812–2819, Nov. 2010.
- [57] J. Vankka, “*Digital Synthesizers and Transmitters for Software Radio*”. Springer, ISBN 978-1-4020-3194-6, 2005.
- [58] V. Parikh, P. Balsara, and O. Eliezer, “A fully digital architecture for wideband wireless transmitters,” in *Radio and Wireless Symposium, 2008 IEEE*, Jan. 2008, pp. 147–150.
- [59] R. Staszewski, J. Wallberg, S. Rezeq, C.-M. Hung, O. Eliezer, S. Vemulapalli, C. Fernando, K. Maggio, R. Staszewski, N. Barton, M.-C. Lee, P. Cruise, M. Entezari, K. Muhammad, and D. Leipold, “All-digital pll and transmitter for mobile phones,” *IEEE J. Solid-State Circuits*, vol. 40, no. 12, pp. 2469–2482, dec. 2005.
- [60] D. M. Pozar, “*Microwave and RF Design of Wireless Systems*”, 1st ed. John Wiley and Sons, 2000.

- [61] R. Schreier, "Noise-shaped coding," Ph.D. dissertation, University of Toronto, Toronto, Canada, May 1991. [Online]. Available: <http://www.dissonance.com/archive/phd/schreier.pdf>
- [62] Z. Song and D. V. Sarwate, "The frequency spectrum of pulse width modulated signals," *Signal Processing*, vol. 83, no. 10, pp. 2227 – 2258, 2003.
- [63] J. Huang, K. Padmanabhan, and O. Collins, "Exact PWM representation of bandlimited signals," in *Information Theory Workshop (ITW), 2010 IEEE*, 30 2010-sept. 3 2010, pp. 1 –5.
- [64] H. Fletcher and W. Munson, "Loudness, its definition, measurement and calculation." *J.Acoust. Soc Am.* 5, pp. 82–108, 1933.
- [65] R. Floyd and L. Steinberg, "An adaptive algorithm for spatial grey scale." *Proc. of the society of Information Display* 17, pp. 75–77, 1976.
- [66] J. Venkataraman and O. Collins, "Continuous waveforms from a binary modulator," in *Signal Processing and Communications, 2004. SPCOM '04. 2004 International Conference on*, dec. 2004, pp. 439 – 443.
- [67] A. Gupta and O. Collins, "Viterbi decoding and sigma-delta modulation," in *Information Theory, 2002. Proceedings. 2002 IEEE International Symposium on*, 2002, p. 292.
- [68] R.-K. Gopalan and O. Collins, "An optimization approach to single-bit quantization," *IEEE Trans. Circuits Syst. I*, vol. 56, no. 12, pp. 2655 –2668, Dec. 2009.
- [69] R. Schreier and G. Temes, "‘*Understanding Delta-Sigma Data Converters*’". New Jersey: Wiley Interscience, 2005.
- [70] J. C. Candy and G. C. Temes, Eds., "‘*Oversampling Delta-Sigma Data Converters Theory, Design and Simulation*’". New York: IEEE Press., 1992.
- [71] R. Norsworthy, R. Schreier, and G. Temes, "‘*Delta-Sigma data converters - Theory, design and simulation*’". New Jersey: Wiley Interscience, 2005.
- [72] H. Inose and Y. Yasuda, "A unity bit coding method by negative feedback," *Proceedings of the IEEE*, vol. 51, no. 11, pp. 1524–1535, Nov. 1963.
- [73] C. Cutler, "Transmission systems employing quantization," *US Patent 2,927,962*, March 8, 1960 (Filed 1954).
- [74] N. Jayant and P. Noll, "‘*Digital coding of waveforms*’". Prentice Hall, Signal Processing Series, ISBN 0-13-211913-7, 1984.
- [75] R. Gray, "Spectral analysis of quantization noise in a single-loop $\Sigma\Delta$ modulator with dc input," *IEEE Trans. Commun.*, vol. 37, no. 6, pp. 588–599, Jun 1989.

- [76] R. Gray, W. Chou, and P. Wong, "Quantization noise in single-loop $\Sigma\Delta$ modulation with sinusoidal inputs," *IEEE Trans. Commun.*, vol. 37, no. 9, pp. 956–968, Sep 1989.
- [77] P. Wong and R. Gray, "Sigma-delta modulation with i.i.d. gaussian inputs," *IEEE Trans. Inf. Theory*, vol. 36, no. 4, pp. 784–798, Jul 1990.
- [78] S. Park and R. Gray, "Sigma-delta modulation with leaky integration and constant input," *IEEE Trans. Inf. Theory*, vol. 38, no. 5, pp. 1512–1533, Sep 1992.
- [79] N. Thao, "Formal spectral theory for ideal $\Sigma\Delta$ quantization with stationary time-varying inputs," *IEEE Trans. Acoust., Speech, Signal Process.*, vol. 3, pp. III–1481–III–1484, April 2007.
- [80] B. Widrow, "A study of rough amplitude quantization by means of nyquist sampling theory," *Circuit Theory, IRE Transactions on*, vol. 3, no. 4, pp. 266–276, Dec 1956.
- [81] W. Bennett, "Spectra of quantized signals." *Bell Syst. Tech. J.*, vol. 27, pp. 446–472, Jul. 1948.
- [82] A. Sripad and D. Snyder, "A necessary and sufficient condition for quantization errors to be uniform and white." *IEEE Trans. Acoust. Speech Signal Proc.*, vol. ASSP-25, pp. 442–448, Oct. 1977.
- [83] R. Gray and A. Gersho, *Vector Quantization and Signal Compression*, 1st ed. Kluwer Academic Press, 1992.
- [84] J. Ostergaard and R. Zamir, "Multiple-description coding by dithered delta $\Sigma\Delta$ quantization," *IEEE Trans. Inf. Theory*, vol. 55, no. 10, pp. 4661–4675, oct. 2009.
- [85] S. Boyd and L. Vandenberghe, "*Convex Optimization*", 1st ed. Cambridge University Press, 2004.
- [86] R. Schreier, "MATLAB Delta Sigma Toolbox," Available at <http://www.mathworks.com/matlabcentral/fileexchange/19>.
- [87] W. Lee and C. Sodini, "A topology for higher order interpolative encoders," vol. 4, May 1987, pp. 459–462.
- [88] K. Chao, S. Nadeem, W. Lee, and C. Sodini, "A higher order topology for interpolative modulators for oversampling a/d conversion." *IEEE Trans. Circuits Syst. I*, vol. 5, no. 37, pp. 309–318, Oct. 1990.
- [89] S. Hein and A. Zakhor, "On the stability of sigma delta modulators," *Signal Processing, IEEE Transactions on*, vol. 41, no. 7, pp. 2322–2348, jul 1993.
- [90] N. Thao, "The tiling phenomenon in $\Sigma\Delta$ modulation," *IEEE Trans. Circuits Syst. I*, vol. 51, no. 7, pp. 1365–1378, July 2004.
- [91] S. Kay, "*Fundamentals of statistical signal processing - Volume 1: Estimation*". New Jersey: Prentice Hall Signal Processing Series, 1993.

- [92] I. Galton, "Delta-sigma data conversion in wireless transceivers," *IEEE Trans. Microw. Theory Tech.*, vol. 50, no. 1, pp. 302 – 315, Jan. 2002.
- [93] A. Jayaraman, P. Chen, G. Hanington, L. Larson, and P. Asbeck, "Linear high-efficiency microwave power amplifiers using bandpass delta-sigma modulators," *IEEE Microw. Guided Wave Lett.*, vol. 8, no. 3, pp. 121 – 123, Mar. 1998.
- [94] T. Blocher and P. Singerl, "Coding efficiency for different switched-mode rf transmitter architectures," *Circuits and Systems, Midwest Symposium on*, vol. 0, pp. 276–279, 2009.
- [95] C. Nzeza, A. Flament, A. Frappe, A. Kaiser, A. Cathelin, and J. Muller, "Reconfigurable complex digital delta-sigma modulator synthesis for digital wireless transmitters," July 2008, pp. 320–325.
- [96] P. Kenington, "RF and Baseband Techniques for Software Defined Radio". Boston: Artech House Publishers, 2005.
- [97] M. Helaoui, S. Hatami, R. Negra, and F. Ghannouchi, "A novel architecture of delta-sigma modulator enabling all-digital multiband multi-standard rf transmitters design," *IEEE Trans. Circuits Syst. II*, vol. 55, no. 11, pp. 1129 –1133, nov. 2008.
- [98] L. Shu-Hsien and Y. Wang, "High efficiency WCDMA power amplifier with pulsed load modulation (PLM)," *IEEE J. Solid-State Circuits*, vol. 45, no. 10, pp. 2030 –2037, Oct. 2010.
- [99] W.-F. Loke, M.-W. Chia, and P.-Y. Chee, "Phase wrapping digital polar transmitter for multi-band OFDM ultra-wideband system," in *Microwave Symposium Digest, 2009. MTT '09. IEEE MTT-S International*, June 2009, pp. 401 –404.
- [100] J. Choi, J. Yim, J. Yang, J. Kim, J. Cha, D. Kang, D. Kim, and B. Kim, "A $\Delta\Sigma$ - Digitized Polar RF Transmitter," *IEEE Trans. Microw. Theory Tech.*, vol. 55, no. 12, pp. 2679–2690, Dec. 2007.
- [101] A. Dupuy and Y. Wang, "High efficiency power transmitter based on envelope $\Delta\Sigma$ modulation (EDSM)," *Vehicular Technology Conference, 2004. VTC2004-Fall. 2004 IEEE 60th*, vol. 3, pp. 2092–2095 Vol. 3, Sept. 2004.
- [102] J. Jinseong and Y. Wang, "A Polar Delta-Sigma Modulation (PDSM) scheme for high efficiency wireless transmitters," in *Microwave Symposium, 2007. IEEE/MTT-S International*, Honolulu, HI, June 2007, pp. 73 – 76.
- [103] P. Aziz, H. Sorensen, and J. V. der Spiegel, "Multi band sigma delta analog to digital conversion," *Acoustics, Speech, and Signal Processing, IEEE International Conference on*, vol. 6, pp. 249–252, 1994.
- [104] T. Kitayabu, Y. Amano, and H. Ishikawa, "Concurrent dual-band transmitter architecture for spectrum aggregation system," in *Radio and Wireless Symposium (RWS), 2010 IEEE*, jan. 2010, pp. 689 –692.

-
- [105] T. Kitayabu and H. Ishikawa, “Generalized architecture of concurrent dual-band transmitter for spectrum aggregation system,” in *Personal Indoor and Mobile Radio Communications (PIMRC), 2010 IEEE 21st International Symposium on*, sept. 2010, pp. 111–116.

